Wave packet interferometry for short-time electronic energy transfer: Multidimensional optical spectroscopy in the time domain

Jeffrey A. Cina,[a] Dmitri S. Kilin, and Travis S. Humble
Department of Chemistry and Oregon Center for Optics, University of Oregon, Eugene, Oregon 97403

(Received 18 July 2002; accepted 16 September 2002)

We develop a wave packet interferometry description of multidimensional ultrafast electronic spectroscopy for energy-transfer systems. After deriving a general perturbation-theory-based expression for the interference signal quadrilinear in the electric field amplitude of four phase-locked pulses, we analyze its form in terms of the underlying energy-transfer wave packet dynamics in a simplified oriented model complex. We show that a combination of optical-phase cycling and polarization techniques will enable the experimental isolation of complex-valued overlaps between a ''target'' vibrational wave packet of first order in the energy-transfer coupling *J*, characterizing the one-pass probability *amplitude* for electronic energy transfer, and a collection of variable ''reference'' wave packets prepared independently of the energy-transfer process. With the help of quasiclassical phase-space arguments and analytic expressions for local signal variations, the location and form of peaks in the two-dimensional interferogram are interpreted in terms of the wave packet surface-crossing dynamics accompanying and giving rise to electronic energy transfer.
 [DOI: 10.1063/1.1519259]

I. INTRODUCTION

Advances in controlling[1,2] or monitoring[3] the interpulse delays within sequences of femtosecond laser pulses with suboptical-period accuracy have triggered the development of new electronic interference spectroscopies in which the signal is quadrilinear in external fields bearing precisely specified optical phase relationships to one another.[4–6] The power of these techniques for elucidating chemical dynamics lies in generating coherent signals that are directly proportional to the overlap between multipulse target and reference nuclear wave packets (in a pure-state description) or to a multipulse density matrix increment (in a mixed-state treatment). This feature stands in contrast to more standard homodyne-detected four-wave mixing spectroscopies, which measure quantities proportional to the absolute-value-squared of the corresponding overlap or density matrix increment and do not require phase-controlled pulse sequences. It also differs from ultrafast pump–probe[7] and time-resolved fluorescence[8] spectroscopies, which are linear in a density matrix increment but *bilinear* in each of two external pulses (pump and probe or gate) and which to first approximation monitor time-dependent nuclear probability densities[9] rather than overlaps between distinct amplitudes. The latter two examples additionally require a compromise between time resolution (pulse duration) and frequency resolution (spectral selectivity) in at least one of the pulses, whereas amplitude-sensitive interference spectroscopy approaches its ideal realization with pulses short enough to freeze nuclear motion on the fastest time scales.

The experimental study of amplitude-sensitive nonlinear electronic spectroscopy was initiated by Wiersma and co-workers with their measurement of phase-locked heterodyne-detected stimulated photon echoes (pl-HSPE) from dye molecules in solution.[4,10] The current state of progress in the field is exemplified by Jonas and co-workers' recent two-dimensional Fourier-transform study of electronic transitions in another solvated laser dye.[6] In addition to incorporating a number of technical improvements, those experiments[6] may reveal additional information about nonresonant effects because they employ an external reference field that does not pass through the sample. There have been parallel advances in heterodyne-detected multidimensional vibrational spectroscopy of both solvated chromophores[11] and neat liquids.[12]

Theory has guided all of these developments. The phase-locked heterodyned photon echo (and the closely related three-pulse phase-locked pump–probe absorption) was suggested by Cho *et al.*[13] Tanimura and Mukamel[14] analyzed the prospects for multidimensional vibrational spectroscopy prior to its successful implementation. Theoretical studies by Metiu and Engel[15] prefigured the original experiments on linear interference spectroscopy with phase-locked pulses.[1,2]

Despite the experimental progress and the contributions from theory in elucidating the physical content of ultrafast electronic interference measurements, much work remains to be done toward interpreting these signals in terms of the underlying molecular processes. In this context, it is desirable to seek detailed pictures of many-body condensed-phase dynamics similar to those that have emerged from relatively simpler pump–probe experiments[16] and time-resolved coherent anti-Stokes–Raman scattering (tr-CARS) signals from chromophores in low-temperature matrices.[17] The most illuminating interpretations in each case have been wave packet descriptions akin to those originally devised for linear absorption[18] and resonance Raman[19] data.[9,20–23]

In previous research that helped develop wave packet pictures for multidimensional interference experiments, we analyzed the ability of nonlinear wave packet interferometry measurements equivalent to the pl-HSPE to prepare and

[a]Electronic mail: cina@oregon.uoregon.edu

measure superpositions between differently handed states in the double-well potential of a chiral molecule.[24] More recently, we have shown that nonlinear wave packet interferometry has the capacity to reveal the complex-valued overlaps between a given short-pulse-generated target wave packet on an excited potential energy surface of a polyatomic molecule and an exhaustive collection of variable reference wave packets.[25,26] Among other uses, this form of wave packet interferometry could serve as a diagnostic tool for quantum control[27] and molecule-based quantum information processing.[28]

Here we make a detailed study of multidimensional time-domain electronic interference spectra for a model complex supporting electronic energy transfer, and interpret their form in terms of the amplitude dynamics of the nuclear wave packets on and between donor-excited and acceptor-excited electronic potential energy surfaces. The ultrafast dynamics of electronic energy transfer in photosynthetic light-harvesting complexes,[29] J-aggregates,[30] and various model complexes[31–34] has been the focus of intensive investigation. This prototypical process in chemical dynamics was described by Förster in an insightful heuristic treatment.[35] A more rigorous treatment, which generalizes the original description by incorporating electronic coherence and inter- as well as intramolecular motion was later put forward by Rackovsky and Silbey[36] and Soules and Duke.[37,38] While the focus in prior studies has mostly been on donor- and acceptor-state population dynamics or nuclear probability densities (proportional to the square and higher even powers of the transfer matrix element J), we show here that wave packet interferometry measurements are sensitive to the nuclear probability amplitude (linear in J) for electronic energy transfer.

The desirability of obtaining amplitude-level dynamical information for energy-transfer systems stems in part from general considerations similar to those that make such information valuable in the simpler context of light-induced nuclear motion within a single electronic state: There is no more complete description of the time development of a system following interaction with an arbitrarily shaped resonant laser pulse than that given by the excited-state nuclear wave function (or density matrix increment). For instance, while it is possible, in principle, to predict the future behavior of a molecule in a given electronic state (or states) from knowledge of the molecular Hamiltonian and nuclear wave function(s) at some instant, the same is not true starting from the Hamiltonian and an initial spatial probability density alone. It can also be argued that, as the most complete possible description of the state of nuclear motion, the time-dependent nuclear wave function should be uniquely sensitive to parameters defining what may be an only approximately known molecular Hamiltonian. The predicted proportionality between the wave packet interferometry signal and the energy-transfer matrix element is a vivid example of the latter feature of amplitude-sensitive measurements.

Within the specific context of energy-transfer systems, for which many conventional experimental methods have been crafted to monitor the change in population of donor and acceptor electronic states, the application of amplitude-sensitive spectroscopies will represent a significant qualitative advance. It has been clear for some time that coherences between electronic states, and hence the nuclear amplitude in those states, can influence the course of electronic energy transfer.[36] Moreover, there is every reason to believe that rational attempts to control the energy transfer process externally in real time will benefit from the development of experimental methods for directly tracking donor-excited and acceptor-excited nuclear wave packets.

Our model energy-transfer complex is a simple one amenable to detailed analysis. It comprises a pair of interacting two-level chromophores whose electronic transition dipole moments are fixed in space. Donor and acceptor chromophores each support a single intramolecular vibration. We touch on the issue of inhomogeneous broadening of the electronic transition frequencies, but defer until later the incorporation of important features such as multiple intra- and intermolecular vibrational modes, orientational disorder, electronic dephasing, and thermal congestion.[39] By illustration with this model complex, we show that nonlinear wave packet interferometry, together with the tools of optical phase control and polarization spectroscopy, is directly sensitive at the amplitude level to the dynamics of internuclear motion accompanying and giving rise to energy-transfer surface-crossing transitions. It has the capacity to monitor the basic process of electronic-nuclear state entanglement that underlies energy transfer, and ameliorates a long-perceived shortcoming of conventional measurements on two-electronic-state systems.[40]

II. BASIC THEORY

We consider a dimer complex whose Hamiltonian,

$$H=|0\rangle H_0\langle 0|+|1\rangle H_1\langle 1|+|1'\rangle H_{1'}\langle 1'|+|2\rangle H_2\langle 2| + J\{|1'\rangle\langle 1|+|1\rangle\langle 1'|\}, \tag{1}$$

comprises four electronic levels: $|0\rangle=|g_a g_b\rangle$ with both molecules unexcited, $|1\rangle=|e_a g_b\rangle$ with the ''donor'' excited, $|1'\rangle=|g_a e_b\rangle$ with the ''acceptor'' excited, and $|2\rangle=|e_a e_b\rangle$ with both molecules excited. The corresponding nuclear Hamiltonians,

$$H_j=\frac{p_a^2}{2m}+\frac{p_b^2}{2m}+\nu_j(q_a,q_b), \tag{2}$$

with potential energy surfaces,

$$\nu_0=\frac{m\omega^2}{2}(q_a^2+q_b^2), \tag{3}$$

$$\nu_1=\epsilon_1+\frac{m\omega^2}{2}((q_a-d)^2+q_b^2), \tag{4}$$

$$\nu_{1'}=\epsilon_{1'}+\frac{m\omega^2}{2}(q_a^2+(q_b-d)^2), \tag{5}$$

$$\nu_2=\epsilon_2+\frac{m\omega^2}{2}((q_a-d)^2+(q_b-d)^2), \tag{6}$$

govern the motion of one intramolecular vibration in each chromophore. The equilibrium position of a vibrational mode

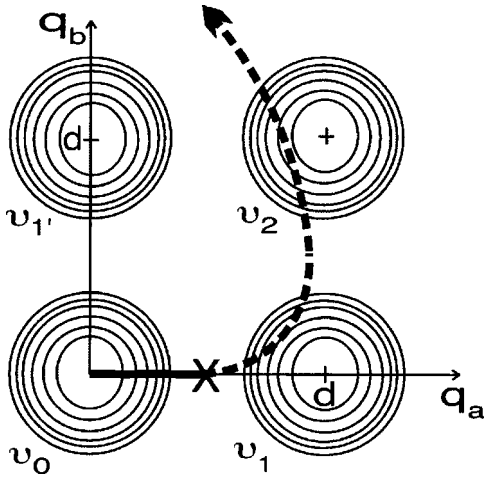

FIG. 1. Schematic contour plots of potential energy surfaces for electronic ground state, donor excited state, acceptor excited state, and two-exciton state. The minimum of energy in each potential is at the corresponding site energy, as in Eqs. (3)–(6). A sketch of the spatial path for a possible contribution to the target wave packet is also shown.

is displaced by a distance d when the host molecule is electronically excited. The site energy of the two-exciton state is typically $\epsilon_2 \cong \epsilon_1 + \epsilon_{1'}$.[41,42]

Figure 1 shows a contour plot of the four site potential energy surfaces.[43] A state change from 1 to $1'$—energy transfer from donor to acceptor—is expected to proceed efficiently at positions where $\nu_1 = \nu_{1'}$. This intersection occurs along a diagonal line $q_b = q_a - (\epsilon_1 - \epsilon_{1'})/m\omega^2 d$ whose location depends on the site-energy difference between donor and acceptor moieties.[44] As energy transfer ensues, an entangled state develops through the process $|1\rangle|\psi_1\rangle \rightarrow |1\rangle|\psi_1\rangle + |1'\rangle|\psi_{1'}\rangle$. While the transferred population, $\langle\psi_{1'}|\psi_{1'}\rangle$, is often measured, and some information about the time evolution of the probability density, $|\psi_{1'}(q_a, q_b)|^2$, has already been obtained from ultrafast experiments, there does not yet appear to have been a direct determination of the entangled state itself, or in particular, of the transferred *amplitude* $|\psi_{1'}\rangle$.

We shall see that wave packet interferometry with optically phase-locked ultrashort-pulse sequences can reveal the complex-valued overlap of a "target" wave packet describing the energy-transfer amplitude with a collection of reference wave packets of specified structure. The ultrashort pulses that generate the target and reference wave packets will be part of a phase-controlled sequence, so we treat the evolution of the system under the time-dependent Hamiltonian $H(t) = H + V_I(t)$, where

$$V_I(t) = -\hat{\boldsymbol{\mu}} \cdot E_I(t), \quad I = A,B,C,D \tag{7}$$

describes the interaction with one of four pulses,

$$E_I(t) = \mathbf{e}_I A_I(t - t_I)\cos(\Omega_I(t - t_I) + \Phi_I), \tag{8}$$

each of which has a well-defined polarization, envelope function, arrival time, carrier frequency, and phase. The intervals between pulses are referred to as $t_p = t_B - t_A$, $t_w = t_C - t_B$, and, $t_d = t_D - t_C$.[45] The electronic dipole moment operator,

$$\hat{\boldsymbol{\mu}} = \boldsymbol{\mu}_a(|1\rangle\langle 0| + |2\rangle\langle 1'|) + \boldsymbol{\mu}_b(|1'\rangle\langle 0| + |2\rangle\langle 1|) + \text{H.c.}, \tag{9}$$

allows transitions in which the exciton number changes by one. For our purposes, it is important that the molecular dipoles be nonparallel, so that pulses of different polarization can selectively address either the donor or the acceptor.

The experimental observable will be the portion of the population of a specific excited electronic state that is *quadrilinear* in the field amplitudes (i.e., proportional to $A_A A_B A_C A_D$) immediately following the four-pulse sequence.[46] To calculate that population, it is sufficient to have the perturbative wave function,

$$|\Psi(t)\rangle = [t - t_D](1 + D)[t_d](1 + C)[t_w] \times (1 + B)[t_p](1 + A)[t_A - t_0]|\Psi(t_0)\rangle, \tag{10}$$

in which the molecular evolution operators[47] are written as $[t] = \exp(-iHt)$ and pulse overlap has been neglected.[48] The operators $I = A$, B, C, and D are pulse propagators,[49]

$$I = -i\int_{-\infty}^{\infty} d\tau[-\tau + t_I]V_I(\tau)[\tau - t_I], \tag{11}$$

whose forms are simplified by neglecting energy transfer during the pulses and adopting the rotating wave approximation.[50]

In calculating the amplitude in each of the excited states, we take note of the fact that an odd number of laser–molecule interactions (one or three) are required to reach either of the one-exciton states, while an even number (two or four) are needed to reach the two-exciton state. For the nuclear wave function in the acceptor-excited state, we find

$$\begin{aligned}|\psi_{1'}(t)\rangle = \langle 1'|[t - t_D]\{&D[t_d + t_w + t_p] + [t_d]C[t_w + t_p] \\ &+ [t_d + t_w]B[t_p] + [t_d + t_w + t_p]A \\ &+ D[t_d]C[t_w]B[t_p] + D[t_d]C[t_w + t_p]A \\ &+ D[t_d + t_w]B[t_p]A \\ &+ [t_d]C[t_w]B[t_p]A\}|0\rangle|n_0\rangle.\end{aligned} \tag{12}$$

Similar expressions can readily be found for the nuclear probability amplitude in the other electronic states.[51]

Since we are interested in the amplitude for $1 \rightarrow 1'$ electronic energy transfer of first order in J, we need to examine the contributions to $|\psi_{1'}\rangle$ that are first and zeroth order in J. The former are possible target wave packets while the latter are available as reference states. Keeping contributions to the free evolution operator that are zeroth and first order in J,[52]

$$[t] = [t]_0 + [t]_1, \tag{13}$$

we can rewrite Eq. (12) as

$$\begin{aligned}|\psi_{1'}(t)\rangle = &|A_{1'}\rangle + |B_{1'}\rangle + |C_{1'}\rangle + |D_{1'}\rangle + |(JA)_{1'}\rangle \\ &+ |(JB)_{1'}\rangle + |(JC)_{1'}\rangle + |(JD)_{1'}\rangle \\ &+ |(DCB)_{1'}\rangle + |(DCA)_{1'}\rangle + |(DBA)_{1'}\rangle \\ &+ |(CBA)_{1'}\rangle + |(JDCB)_{1'}\rangle + |(DCJB)_{1'}\rangle \\ &+ |(JDCA)_{1'}\rangle + |(DCJA)_{1'}\rangle + |(JDBA)_{1'}\rangle \\ &+ |(DBJA)_{1'}\rangle + |(JCBA)_{1'}\rangle + |(CBJA)_{1'}\rangle,\end{aligned} \tag{14}$$

which uses the short-hand notation

$$|(DCJB)_{1'}\rangle = \langle 1'|[t-t_D]_0 D[t_d]_0 C[t_w]_1 B[t_p]_0|0\rangle|n_0\rangle, \tag{15}$$

and so forth.

In order to calculate the interference population $P_{1'}$, we must identify the quadrilinear contributions[53] to $\langle\psi_{1'}|\psi_{1'}\rangle$: a sum of four terms that are zeroth order in J (e.g., $2\,\mathrm{Re}\langle(DCB)_{1'}|(A)_{1'}\rangle$) and twelve terms that are first order in J (e.g., $2\,\mathrm{Re}\langle(DCB)_{1'}|(JA)_{1'}\rangle$).[54] But the situation can simplify considerably when we take account of laser polarization, as each of the amplitudes in Eq. (14) depends on the relative orientation of the field polarizations and molecular dipole moment operators.[55]

III. CASE STUDY

We consider a simple example illustrating some basic features of interference measurements of energy transfer: the dimer is assigned a well-defined internal and lab-frame geometry—as in a cryogenic matrix, macromolecular crystal, or layered structure[56]—with $\boldsymbol{\mu}_a = \mu\mathbf{i}$ and $\boldsymbol{\mu}_b = \mu\mathbf{j}$ along the *space-fixed* x and y axes, respectively. Then x-polarized pulses can drive the transitions

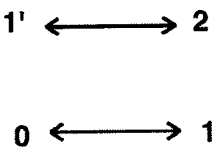

(16)

while y-polarized pulses drive the transitions

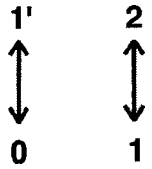

(17)

Target amplitude on the acceptor state of first order in J can result from energy transfer following excitation of the donor state by an x-polarized laser pulse:

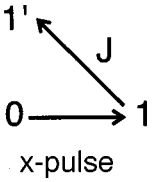

(18)

Preparation of a reference wave packet (zeroth order in J) that can interfere with this $1'$ target requires one (or three) y-polarized pulses and two (or no) x-polarized pulses. The former case (with a total of three x-polarized pulses and one y-polarized pulse) is suitable for our purposes, as it affords a wide variety of reference packets with both modes of vibration set in motion. This feature is useful in generating overlap with a target state whose a mode is set moving after short-pulse excitation of the donor and whose b-mode motion is initiated by energy transfer.

We consider four different polarization combinations: $A_yB_xC_xD_x$, $A_xB_yC_xD_x$, $A_xB_xC_yD_x$, and $A_xB_xC_xD_y$. Under the first of these, the acceptor-state amplitude reduces to

$$|\psi_{1'}(t)\rangle = \left|(A_y)_{1'}\right\rangle + \left|(JB_x)_{1'}\right\rangle + \left|(JC_x)_{1'}\right\rangle + \left|(JD_x)_{1'}\right\rangle$$

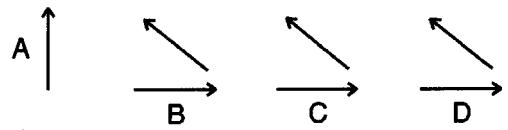

$$+ \left|(D_xC_xA_y)_{1'}\right\rangle + \left|(D_xB_xA_y)_{1'}\right\rangle + \left|(C_xB_xA_y)_{1'}\right\rangle$$

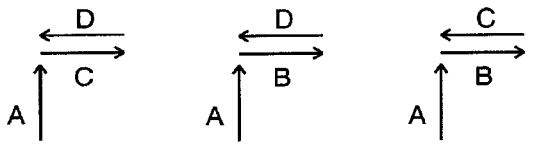

$$+ \left|(JD_xC_xB_x)_{1'}\right\rangle + \left|(D_xC_xJB_x)_{1'}\right\rangle$$

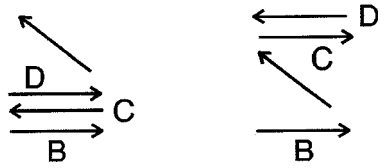

(19)

The resulting quadrilinear contribution to $\langle\psi_{1'}(t)|\psi_{1'}(t)\rangle$ specifies the interference contribution to the acceptor-excited state population:

$$\begin{aligned} P_{1'}(A_yB_xC_xD_x) = 2\,\mathrm{Re}\{&\langle(A_y)_{1'}|(JD_xC_xB_x)_{1'}\rangle \\ &+\langle(A_y)_{1'}|(D_xC_xJB_x)_{1'}\rangle \\ &+\langle(D_xC_xA_y)_{1'}|(JB_x)_{1'}\rangle \\ &+\langle(D_xB_xA_y)_{1'}|(JC_x)_{1'}\rangle \\ &+\langle(C_xB_xA_y)_{1'}|(JD_x)_{1'}\rangle\}. \end{aligned} \tag{20}$$

As expected, this signal contains no terms of zeroth order in J.

It is useful to consider specific values of the relative optical phases of the pulses. Under a generalization of the phase-locking scheme developed by Scherer and co-workers for linear wave packet interferometry with phase-locked pulse pairs,[1,2] it is possible[4] to make sequences of the form (8) comprising *pairs* of pulse-pairs AB and CD for which

$$\Phi_B = \Phi_A + \Omega_p t_p + \phi_p, \quad \Phi_D = \Phi_C + \Omega_d t_d + \phi_d, \tag{21}$$

respectively. The phase shift $\phi_p(\phi_d)$ is termed the locking angle of the AB (CD) pulse pair at the locking frequency $\Omega_p(\Omega_d)$. The *interpulse-pair* phase shifts need not be controlled, so for our purposes angles such as $\Phi_C - \Phi_B$ may be formally assumed to sample a full range of values from 0 to 2π over many laser shots.[57]

Expressions (7), (8), and (11) show that parts of a pulse propagator I which induce upward transitions (proportional to $|1\rangle\langle 0|$, $|1'\rangle\langle 0|$, $|2\rangle\langle 1|$, and $|2\rangle\langle 1'|$) contain a phase factor $\exp(-i\Phi_I)$. Parts of I that induce downward transitions (proportional to $|0\rangle\langle 1|$, $|0\rangle\langle 1'|$, $|1\rangle\langle 2|$, and $|1'\rangle\langle 2|$) contain a

phase factor $\exp(i\Phi_I)$. As a result, we see that the last two terms in Eq. (20) are not phase controlled and hence average to zero over many repetitions. Using the optical phases (21), we find that

$$P_{1'}(\phi_p,\phi_d)=2\,\mathrm{Re}\{\exp(-i\phi_p-i\phi_d)\times(\langle(A_y)_{1'}|(JD_xC_xB_x)_{1'}\rangle^{(0)}+\langle(D_xC_xA_y)_{1'}|(JB_x)_{1'}\rangle^{(0)})+\exp(-i\phi_p+i\phi_d)\langle(A_y)_{1'}|(D_xC_xJB_x)_{1'}\rangle^{(0)}\},\quad(22)$$

in which the superscript (0) designates the overlap with both pulse pairs in-phase (i.e., $\phi_p=\phi_d=0$). While three distinct overlaps can contribute to the interference signal (22) for an arbitrary choice of the phase-locking angles, it is possible to combine signals with different phase shifts in order to isolate the combinations

$$\langle(A_y)_{1'}|(JD_xC_xB_x)_{1'}\rangle^{(0)}+\langle(D_xC_xA_y)_{1'}|(JB_x)_{1'}\rangle^{(0)}=\frac{1}{4}\left\{P_{1'}(0,0)+P_{1'}\left(\frac{\pi}{2},-\frac{\pi}{2}\right)+iP_{1'}\left(\frac{\pi}{2},0\right)+iP_{1'}\left(0,\frac{\pi}{2}\right)\right\}\quad(23)$$

and

$$\langle(A_y)_{1'}|(D_xC_xJB_x)_{1'}\rangle^{(0)}=\frac{1}{4}\left\{P_{1'}(0,0)-P_{1'}\left(\frac{\pi}{2},-\frac{\pi}{2}\right)+iP_{1'}\left(\frac{\pi}{2},0\right)-iP_{1'}\left(0,\frac{\pi}{2}\right)\right\}.\quad(24)$$

Combining signals with different values of ϕ_p and ϕ_d by the prescriptions (23) and (24) is an example of "phase cycling" in optical spectroscopy.[58,59] Equation (24) illustrates a key prediction of our analysis, that nonlinear wave packet interferometry with pairs of pulse pairs is capable of isolating the full complex overlap[60] $\langle\alpha_{1'}|\xi_{1'}\rangle=\langle(A_y)_{1'}|(D_xC_xJB_x)_{1'}\rangle^{(0)}$ between a given energy-transfer target

$$|\xi_{1'}\rangle=\exp(i\Phi_B)\langle 1'|[t_w]_1B_x|0\rangle|n_0\rangle,\quad(25)$$

generated by first-order energy transfer during t_w, and the members of a collection of variable reference wave packets

$$|\alpha_{1'}\rangle=\{\exp(i\Phi_B)\langle 1'|C_x^\dagger[-t_d]_0D_x^\dagger[t_d+t_w+t_p]_0A_y\times[-t_p]_0|0\rangle|n_0\rangle\}|_{\phi_p=\phi_d=0}.\quad(26)$$

The C and D pulse propagators are reassigned to the reference wave packet in Eq. (26) in order to highlight the correspondence between Eqs. (25) and (18); some phase factors have been introduced in both bra and ket to render the target wave packet independent of t_p and ϕ_p. Notice that the reference state evolves *backwards* in the two-exciton state during t_d.

The remaining polarization combinations of immediate interest are considered in Appendix A. A complete scan of interpulse delays would also include the two interleaved pulse sequences *ACBD* and *ACDB*; these alternative orderings provide some interesting overlaps, but we do not pause to analyze them here. The analysis of this section has focused on isolating a particular contribution to $P_{1'}$, the quadrilinear acceptor-excited state population. Section V will address some practical issues associated with measuring $P_{1'}$ itself, by polarized fluorescence for example, in the presence of possible quadrilinear populations in the other excited states 1 and 2.

IV. ENERGY-TRANSFER WAVE PACKET DYNAMICS

A quasiclassical analysis of phase-space trajectories can indicate when the overlap $\langle\alpha_{1'}|\xi_{1'}\rangle$, experimentally isolable according to Eq. (24), should be nonvanishing. A schematic trajectory for the dominant portions of the target wave packet $|\xi_{1'}\rangle$ is shown in Fig. 2. We specialize to energy-transfer waiting times equal to half a vibrational period, $t_w=\tau_{\mathrm{vib}}/2=\pi/\omega$, in order to allow time for only one crossing of the intersection between the $\nu_1(q_a,q_b)$ and $\nu_{1'}(q_a,q_b)$ surfaces, and show the average values of *a*-mode and *b*-mode position and momentum that should result when the energy-transfer transition from 1 to $1'$ occurs after αt_w in state 1. After the surface-crossing transition, the *a*-mode trajectory sweeps out an angle $\pi(1-\alpha)$ about $(\omega q_a,\dot{q}_a)=(0,0)$; this is *twice* the angular displacement about the same origin that would have occurred if energy transfer had not taken place.[61,62] Meanwhile, the *b*-mode undergoes an angular displacement by $\pi(1-\alpha)$ about $(\omega q_b,\dot{q}_b)=(\omega d,0)$ after energy transfer.

A schematic diagram of the phase-space motion for the reference wave packet $|\alpha_{1'}\rangle$ is shown in Fig. 3. In order for the target and reference wave packets to overlap significantly, their phase-space coordinates must nearly coincide. Comparison with Fig. 2 indicates that sizable overlap should occur for

$$t_p=\left(m+1-\frac{\alpha}{2}\right)\tau_{\mathrm{vib}}.\quad(27)$$

and

$$t_d=\left(n+\frac{\alpha}{2}\right)\tau_{\mathrm{vib}},\quad(28)$$

where m and n are non-negative integers.

It is possible to obtain a closed-form expression for the isolable overlap (24) in the short-pulse limit (pulse duration much less than the inverse absorption bandwidth or inverse Franck–Condon energy). Analytic forms are given in Appendix B for the target (B5) and reference (B7) wave packets; from the commutation properties of harmonic oscillator creation and annihilation operators, we find their overlap

$$\langle\alpha_1|\xi_{1'}\rangle=\langle(A_y)_{1'}|(D_xC_xJB_x)_{1'}\rangle^{(0)}=iJ\left(\frac{\mu}{2}\right)^4\mathrm{area}_A\,\mathrm{area}_B\,\mathrm{area}_C\,\mathrm{area}_D\times e^{i(\epsilon_{1'}-\Omega_p)t_p+i\,(\epsilon_{1'}-\epsilon_2+\Omega_p)t_d}\times\int_0^{\tau_{\mathrm{vib}}/2}d\tau\exp\{i(\epsilon_{1'}-\epsilon_1)\tau+\delta^2e^{i\omega\tau}\times(e^{i\omega t_p}+e^{-i\omega t_d}-1)+\delta^2e^{-i\omega\tau}-2\delta^2\}.\quad(29)$$

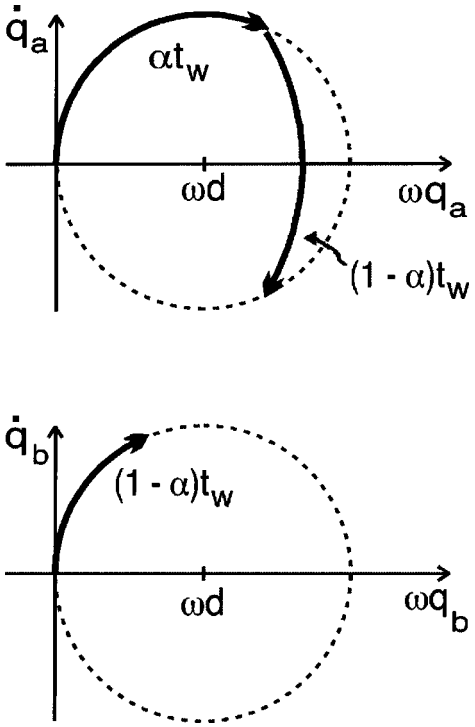

FIG. 2. Phase-space trajectories for the *a*-mode (above) and *b*-mode (below) of a target wave packet prepared by an *x*-polarized *B* pulse. $1' \leftarrow 1$ energy transfer is shown occurring after αt_w of motion in the donor-excited state.

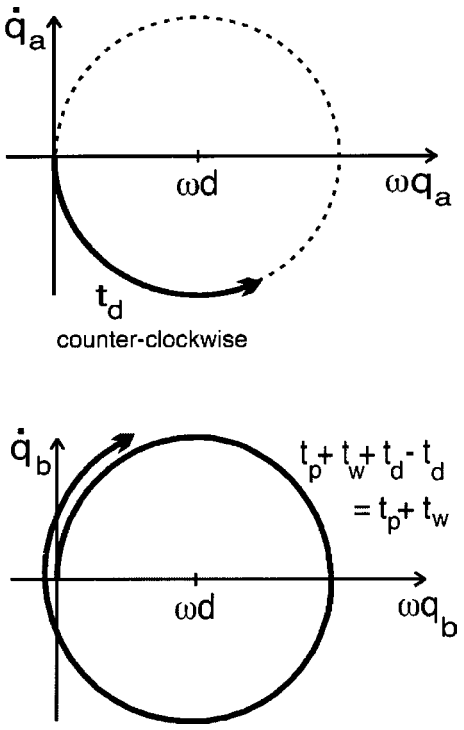

FIG. 3. Phase-space trajectories for the *a*-mode (above) and *b*-mode (below) of a reference wave packet prepared by A_y, C_x, and D_x pulses. The last two pulses operate in reverse order, with an interval t_d of backward evolution between them.

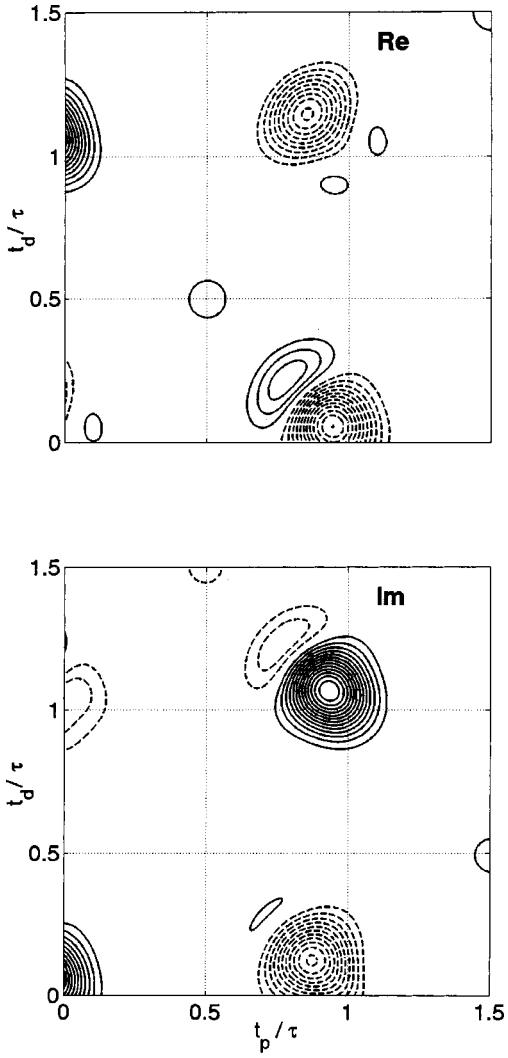

FIG. 4. Calculated interferogram for the case of equal site energies, $\epsilon_1 = \epsilon_{1'}$, and energy-transfer waiting time $t_w = \tau_{\text{vib}}/2$. The sign and size of both the real part and the imaginary part are physically meaningful, giving the complex-valued overlap (29) [divided by $J(\mu/2)^4 \text{area}_A\, \text{area}_B\, \text{area}_C\, \text{area}_D \tau_{\text{vib}}$] as a function of the intrapulse-pair delays t_p and t_d. Positive (negative) contours are given by solid (dashed) lines spaced by 0.008 373, with a maximal (minimal) value $+(-)0.125\,594$.

The pulse areas, area_I, and dimensionless displacement, δ, are as defined in Appendix B.

A. Calculated interferograms

For chosen parameter values, Eq. (29) can be evaluated easily by numerical integration. We take $\omega = 8.3 \times 10^{-4}$ a.u. $\cong 2\pi c(182.17\ \text{cm}^{-1})$, $m = 99\,000$ a.u. $\cong 53.917$ u, $d = 0.3$ a.u. $\cong 0.158\,75$ Å ($\delta^2 = 0.369\,765 = E_{\text{FC}}/\omega$, where $E_{\text{FC}} = m\omega^2 d^2/2$ is the Franck–Condon energy). Both phase-locking frequencies [see Eq. (21)] are chosen to match the vertical transition energy for donor excitation ($\Omega_p = \Omega_d = \epsilon_1 + E_{\text{FC}}$). Figure 4 shows the calculated two-dimensional (2D) interferogram for the case of equal site energies $\epsilon_{1'} = \epsilon_1$. The interferogram for a downhill case with $\epsilon_{1'} = \epsilon_1 - 2E_{\text{FC}}$ is shown in Fig. 5.[63]

The locations of maximal interference signal are in qualitative accord with the quasiclassical predictions of Eqs. (27) and (28) for both equal-energy and downhill cases. For

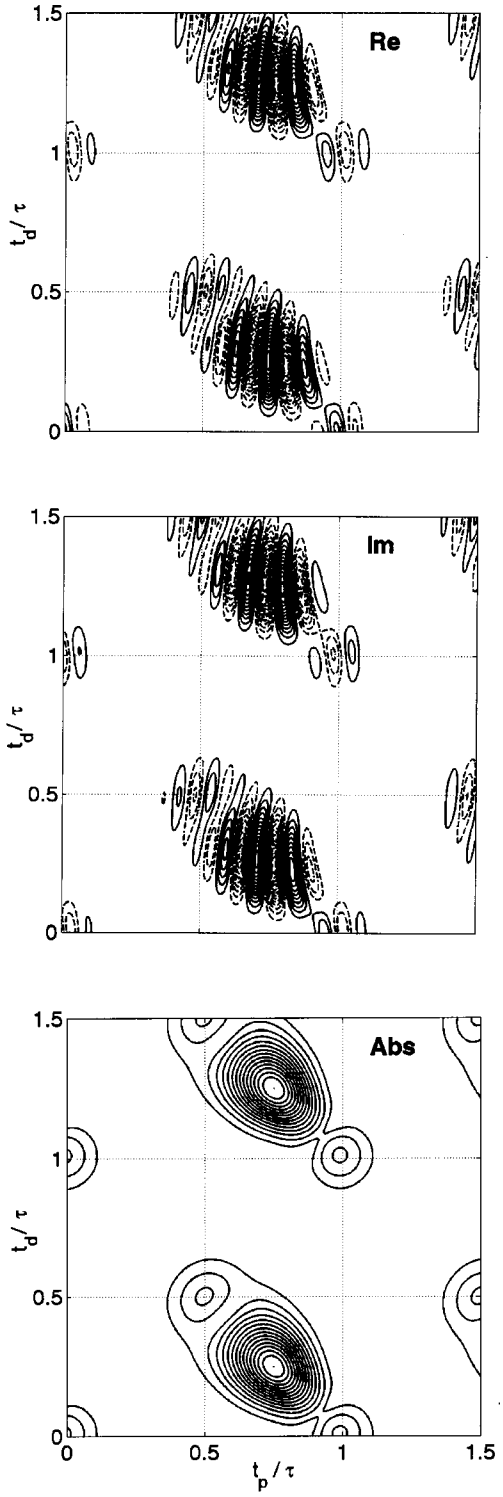

FIG. 5. Calculated interferogram for the case of downhill energy transfer. Same parameters as in Fig. 4 except $\epsilon_{1'}=\epsilon_1-2E_{\mathrm{FC}}$. Also shown is the absolute signal intensity, in which the temporal locations of certain satellite peaks are readily discernible.

the equal-energy interferogram, maxima in $|\langle\alpha_{1'}|\xi_{1'}\rangle|$ are found when $t_p=(m+1-0.155/2)\tau_{\mathrm{vib}}$ and $t_d=(n+0.155/2)\tau_{\mathrm{vib}}$. Maximal signals in the downhill interferogram occur farther "off diagonal," when $t_p=(m+1-0.5/2)\tau_{\mathrm{vib}}$ and $t_d=(n+0.5/2)\tau_{\mathrm{vib}}$. The deviation of the effective energy transfer time $\alpha\tau_{\mathrm{vib}}/2$ from zero in the case of equal site energies can be attributed to the finite time required for the quantum mechanical target wave packet to leave the potential-crossing line at the Franck–Condon point.

The fringe structure in the 2D interferograms of Figs. 4 and 5 reveals amplitude-level information about the form and dynamics of the corresponding target wave packets. The rates of change with t_p and t_d of the phase $\Gamma=-i\ln\langle\alpha_{1'}|\xi_{1'}\rangle$ are given in Eq. (C7) [or (C9)] and Eq. (C8) [or (C10)], respectively (see Appendix C). The last term on the right-hand side of both Eqs. (C7) and (C8), involving the position matrix elements $\langle\alpha_{1'}|q_b-\overline{q_b}|\xi_{1'}\rangle$ and $\langle\alpha_{1'}|q_a-\overline{q_a}|\xi_{1'}\rangle$, respectively, would vanish if the reference wave packet were the same as the target within a constant factor, as would be expected at the signal maxima in the limit of quasiclassical target-state dynamics ($E_{\mathrm{FC}}\gg\omega$).

The fringe structure of the peaks in Fig. 4 corresponds to $\partial\Gamma/\partial t_p=-\partial\Gamma/\partial t_d\cong-0.53\omega$ at the signal maxima, and these values imply

$$\langle\alpha_{1'}|q_a-\overline{q_a}|\xi_{1'}\rangle=-\langle\alpha_{1'}|q_b-\overline{q_b}|\xi_{1'}\rangle \cong 0.53\frac{\langle\alpha_{1'}|\xi_{1'}\rangle}{m\omega d}e^{i2\pi(0.0775)}$$

for the case of equal site energies. The phase derivatives at the signal maxima in Fig. 5 are $\partial\Gamma/\partial t_p\cong-7.53\omega$ and $\partial\Gamma/\partial t_d\cong 0.14\omega$. Equations (C7) and (C8) in our case of downhill energy transfer then yield

$$\langle\alpha_{1'}|q_a-\overline{q_a}|\xi_{1'}\rangle=-\langle\alpha_{1'}|q_b-\overline{q_b}|\xi_{1'}\rangle \cong 0.14i\frac{\langle\alpha_{1'}|\xi_{1'}\rangle}{m\omega d},$$

a smaller (but still non-negligible) deviation from quasiclassical behavior than in the equal-energy case.

B. Target and reference wave packets

In order to clarify the relationship between the experimentally measurable overlap $\langle\alpha_{1'}|\xi_{1'}\rangle$ and the spatial form of the target and reference wave packets, we have calculated the target wave packet using Eq. (B5) and the reference with which it interferes at intrapair delays producing maximal overlap using Eq. (B7). These are shown in Figs. 6 and 7 for the case of equal site energies and Figs. 8 and 9 for downhill energy transfer. The target wave packet plotted as a function of (q_a,q_b) is seen to bear a discernible resemblance to any single peak in the corresponding interference signal plotted with respect to (t_d,t_p) (i.e., transposed about the diagonal from our Figs. 4 and 5), especially in the equal-energy case. While this vivid correspondence is a feature of the two-vibration model, it serves to illustrate that the 2D interferograms are sensitive records of the energy-transfer surface crossing *amplitude*.

Sources for detailed features in the wave packet interferometry signals of Figs. 4 and 5 can be identified in the corresponding target amplitudes of Figs. 6 and 8, respectively. For instance, the temporally varying signal oscillation frequency observed in Fig. 4 can be attributed in part to the spatially varying local de Broglie wavelengths seen in Fig. 6. The equal energy interferogram (Fig. 4) exhibits small satel-

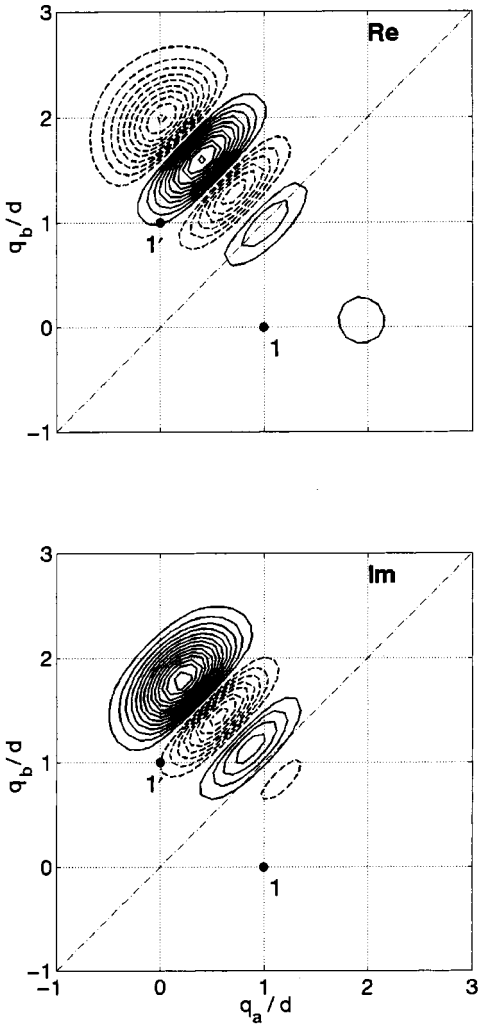

FIG. 6. Real and imaginary parts of the target wave packet for the equal energy case. Equation (B5) is plotted as $\langle q_a, q_b | \xi_{1'} \rangle$ divided by $J(\mu/2)^2 \text{area}_B \tau_{\text{vib}}/d$. Contour lines of the same sign are spaced by 0.013 151 and take maximal (minimal) values $+(-)0.197\,261$. Locations of potential minima for donor-excited (1) and acceptor-excited (1′) states are also shown, as is the line of intersection between ν_1 and $\nu_{1'}$.

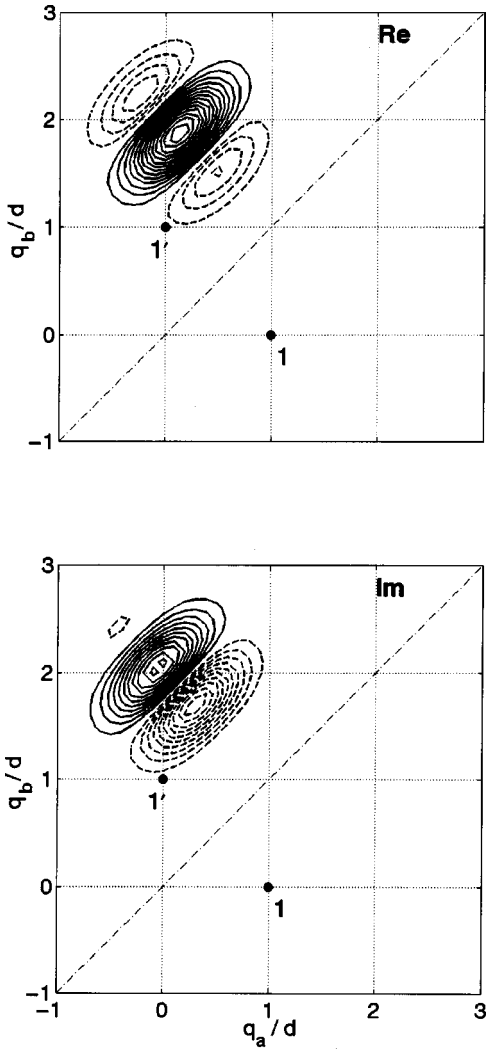

FIG. 7. Real and imaginary parts of the reference wave packet for the equal energy case at $(t_p, t_d)_{\max} = (0.9225, 1.0775)\tau_{\text{vib}}$ Equation (B7) is plotted as $\langle q_a, q_b | \alpha_{1'} \rangle$ divided by $(\mu/2)^3 \text{area}_A \text{ area}_C \text{ area}_D/d$. Contours of the same sign are spaced by 0.102 27 and take maximal (minimal) values $+(-)1.534\,11$.

lite peaks near $(t_p, t_d) = (m+0.5, n+0.5)\tau_{\text{vib}}$. Phase-space diagrams make it clear that reference wave packets prepared with these delays (not shown) will overlap the small trailing region of target amplitude near $(q_a, q_b) = (2d, 0)$ that is visible in Fig. 6. This trailing region of target probability amplitude arises from nonresonant electronic energy transfer late in the waiting period. The wave packet launched by the B_x pulse reaches the outer q_a turning point on the donor-excited surface after half a period, and amplitude transfer can occur because the wave packet lingers there for a time $\sim 2\pi/E_{\text{FC}}$, which is only slightly longer than the local electronic nutation period $2\pi/(\nu_{1'} - \nu_1) \sim 2\pi/4E_{\text{FC}}$.

There is also a series of satellite peaks near $(t_p, t_d) = (m+0.5, n+0.5)\tau_{\text{vib}}$ in the downhill interferogram of Fig. 5. These derive only in part from electronic nutation at the outer a-mode turning point [with local period $2\pi/(\nu_{1'} - \nu_1) \sim 2\pi/2E_{\text{FC}}$, somewhat longer than in the equal-energy case]. In the downhill case, the edge of the donor-excited wave packet prepared by the B_x pulse still penetrates the $\nu_1 = \nu_{1'}$ crossing region in the vicinity of $(q_a, q_b) = (3d/2, d/2)$ as the packet reaches the outer turning point, and resonant energy transfer ensues. Both of these processes contribute to the trailing region of target probability amplitude near $(q_a, q_b) \approx (2d, 0)$ in Fig. 8 and the corresponding satellites in the interferogram. The downhill interferogram has additional satellite peaks near $(t_p, t_d) = (m, n)\tau_{\text{vib}}$. These come once again from both nonresonant electronic nutation [near $(q_a, q_b) = (0,0)$] and resonant transfer [for $(q_a, q_b) \approx (d/2, -d/2)$] when the B_x wave packet is in the Franck–Condon region. The resulting contributions to the target wave packet evolve as a leading region of probability amplitude that is localized between $(q_a, q_b) = (0, 2d)$ and $(q_a, q_b) = (-d/2, 5d/2)$ by the end of the waiting period.

V. DISCUSSION

A. Measuring $P_{1'}$

In Sec. III and Appendix A, we determined the contributions to $P_{1'}(ABCD)$, that are isolable by phase cycling un-

der various polarization combinations. While $P_{1'}$ is independently observable in the sense of being the expectation value of the Hermitian operator $|1'\rangle\langle 1'|$ (or the quadrilinear contribution to that quantity), we still need to consider how it could be measured in practice.

One strategy would be to monitor the time- and frequency-integrated *y*-polarized emission from $1' \rightarrow 0$. But any quadrilinear contribution to the population of the two-exciton state 2 could give rise to *y*-polarized $2 \rightarrow 1$ emission that would obscure the sought-for signal. This complication can perhaps be overcome by the simple expedient of spectrally filtering the *y*-polarized emission. While we have assumed that $\epsilon_2 = \epsilon_1 + \epsilon_{1'}$ in our calculations, this is an inessential choice not strictly obeyed in practice. In actuality, the peak frequency of relaxed emission from the acceptor chromophore will depend slightly on whether the acceptor molecule is or is not electronically excited. Thus *y*-polarized emission from $P_{1'}$ and P_2 should be spectrally distinguishable.

Spectral filtration of the emitted light may not be necessary in the case of downhill energy transfer, however. In this case *x-polarized* emission can serve as an independent measure of the relevant contribution to P_2 under $A_y B_x C_x D_x$. With these polarizations, the amplitudes that overlap to produce a quadrilinear contribution to the population of state 2 result from the electronic transitions

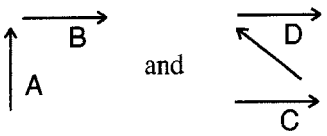

and

not phase locked

(30)

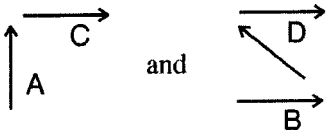

and

$\exp\{-i(\phi_p + \phi_d)\}$

(31)

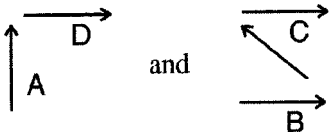

and

$\exp\{-i(\phi_p - \phi_d)\}$

(32)

The phase structure of each term is indicated; there is no contribution to P_2 of zeroth order in J.

We showed in Sec. III that phase-cycling selection of the signal proportional to $\exp(-i\phi_p + i\phi_d)$ could be used to extract the single overlap $\langle (A_y)_{1'} | (D_x C_x J B_x)_{1'} \rangle^{(0)}$ from the other contributions to $P_{1'}$. Expression (32) shows, though, that a portion of P_2 with the same optical phase could make an additional contribution to *y*-polarized emission. State 2 can also emit with *x* polarization, and we can check the phase structure of the quadrilinear *x*-emitting *donor* state population, $P_1(A_y B_x C_x D_x)$, to see whether an $\exp(-i\phi_p + i\phi_d)$ term exists there as well. It happens that two contributions to $P_1(A_y B_x C_x D_x)$, those arising from overlaps between the amplitudes,

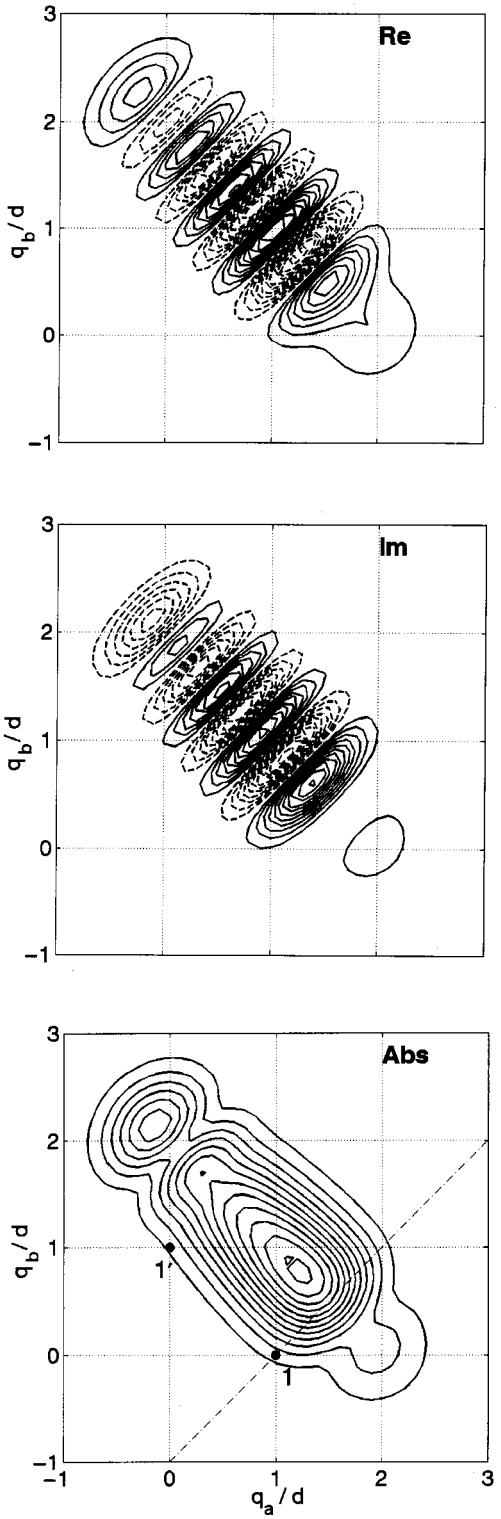

FIG. 8. Same as Fig. 6, but for the downhill case. The absolute value of the target wave packet is also plotted in order to emphasize the spatial locations of local maxima in the probability amplitude due to nonresonant electronic nutation and resonant transfer from the edges of the nuclear wave packet. Both of these secondary energy-transfer mechanisms proceed efficiently at the inner and outer turning points of motion in the donor-excited potential well.

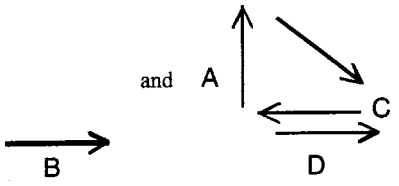

(33)

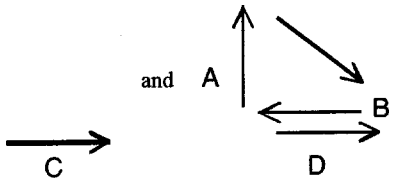

(34)

both carry an $\exp(-i\phi_p - i\phi_d)$ phase factor; so phase selection of the *x*-polarized emission would not generally give an unobscured view of the $\exp(-i\phi_p + i\phi_d)$ contribution to P_2. But the overlap (33) and (34) involve *backward* energy transfer from the acceptor to the donor. If the acceptor site energy is sufficiently far below that of the donor (as in our downhill case, where the acceptor-excited Franck–Condon point is itself E_{FC} below the intersection energy between $\nu_{1'}$ and ν_1), the backwards transition cannot occur for energetic reasons, and the corresponding contribution to P_1 vanishes. Thus for the downhill case, the $\exp(-i\phi_p + i\phi_d)$ component of P_2 can be determined as the sole contribution to *x*-polarized emission having this phase signature. Having been determined independently, this P_2 contribution can be unambiguously removed from the *y*-polarized emission without spectral filtration, leaving the sought-for overlap $\langle (A_y)_{1'} | (D_x C_x J B_x)_{1'} \rangle^{(0)}$ as the only remaining signal.

B. Prospects for state determination

The collection of reference wave packets (26) available under $A_y B_x C_x D_x$ polarization is limited to both *a*-mode and *b*-mode Franck–Condon energy shells (see Fig. 3). The interpair delay $t_w = \tau_{\mathrm{vib}}/2$ places the target (25) on the same energy shell, allowing sizable overlap. Since reference packet formation occurs first on the $\nu_{1'}$ surface (where only q_b is displaced) and then on ν_2 (where both q_a and q_b are displaced), the prospects for determining overlaps with an exhaustive collection of reference packets—including many with average energy *off* the Franck–Condon shell—might appear dim. But measuring overlaps between target wave packets with t_w slightly different from $\tau_{\mathrm{vib}}/2$ and on-shell reference packets can be nearly equivalent to measuring overlaps between targets with $t_w = \tau_{\mathrm{vib}}/2$ and off-shell reference wave packets.

To exhibit this equivalence we note that

$$[t_w + \delta t_w]_1 = [\delta t_w]_0 [t_w]_1 + [\delta t_w]_1 [t_w]_0 \tag{35}$$

(see Ref. 52). For slight increments in waiting time, the second term in Eq. (35) can be neglected (unless $\epsilon_1 - \epsilon_{1'} \cong 4E_{\mathrm{FC}}$, a still greater energy difference than in our downhill case), and

$$\begin{aligned}
\langle \alpha_{1'} | \xi_{1'} \rangle |_{t_w + \delta t_w} &= \langle n_0 | \langle 0 | A_y^\dagger [-t_p - t_w - \delta t_w - t_d]_0 \\
&\quad \times D_x [t_d]_0 C_x | 1' \rangle \langle 1' | [t_w + \delta t_w]_1 \\
&\quad \times B_x [t_p]_0 | 0 \rangle | n_0 \rangle \\
&\cong \langle n_0 | \langle 0 | A_y^\dagger [-t_p - t_w - \delta t_w - t_d]_0 \\
&\quad \times D_x [t_d]_0 C_x [\delta t_w]_0 | 1' \rangle \\
&\quad \times \langle 1' | [t_w]_1 B_x [t_p]_0 | 0 \rangle | n_0 \rangle \\
&= \langle \overline{\alpha}_{1'} | \xi_{1'} \rangle |_{t_w}.
\end{aligned} \tag{36}$$

The effective reference wave packet $|\overline{\alpha}_{1'}\rangle$ of Eq. (36) follows a phase-space trajectory that lies off the Franck–Condon shell for the internal vibration of the donor, increasing the dimensionality of the accessible *a*-mode phase space from one to two. This is a step toward providing an exhaustive set of reference wave packets to interfere with the target packet. To gain a second dimension in the *b*-mode space may require additional optical transitions to access state-0 or state-1 surfaces during reference state preparation.

C. Echolike versus nonecholike signals

When experiments of the kind considered here are carried out on chromophores in low-temperature solids, it will be necessary to consider the effects of inhomogeneous broadening. As a result of differences in local environment, the site energies ϵ_1, $\epsilon_{1'}$, and ϵ_2 in Eqs. (3) through (6) may vary with location in the sample. This spatial inhomogeneity in the site energies could affect the nonlinear wave packet interferometry signal from a bulk sample,[64] but in energy-transfer systems, the effects of inhomogeneity would depend on the degree of correlation between donor and acceptor energy shifts.

The simplest situation would entail perfect correlation between donor and acceptor site energies, so that $\epsilon_1 = \overline{\epsilon_1} + \delta\epsilon$, $\epsilon_{1'} = \overline{\epsilon}_{1'} + \delta\epsilon$, and $\epsilon_2 = \overline{\epsilon_2} + 2\,\delta\epsilon$. In this case, the single overlap (24) that is isolable under $A_y B_x C_x D_x$ polarization depends on the site-energy shift as

$$\langle (A_y)_{1'} | (D_x C_x J B_x)_{1'} \rangle^{(0)} \propto \exp\{ i\,\delta\epsilon (t_p - t_d) \}, \tag{37}$$

and the overlap that is isolable under $A_x B_y C_x D_x$ polarization [see Eq. (A3)] goes as

$$\langle (B_y)_{1'} | (D_x C_x J A_x)_{1'} \rangle^{(0)} \propto \exp\{ -i\,\delta\epsilon (t_p + t_d) \}. \tag{38}$$

In this limiting situation, we would naturally identify the overlaps (37) and (38) as arising from echolike and nonecholike signals, respectively; the former overlap suppresses the effects of (correlated) inhomogeneous broadening along the $t_d \approx t_p$ diagonal and the latter does not.[65]

Dynamical considerations come into play as well, however. The semiclassical criteria (27) and (28) suggest that the overlap $\langle (A_y)_{1'} | (D_x C_x J B_x)_{1'} \rangle^{(0)}$ can be nonzero when the delay difference in Eq. (37) takes on values

$$t_p - t_d = (m - n + 1 - \alpha)\,\tau_{\mathrm{vib}}, \tag{39}$$

some or all of which may appear off the diagonal. On the other hand, Eq. (A7) indicates that $\langle (B_y)_{1'} | (D_x C_x J A_x)_{1'} \rangle^{(0)}$ can be nonzero when

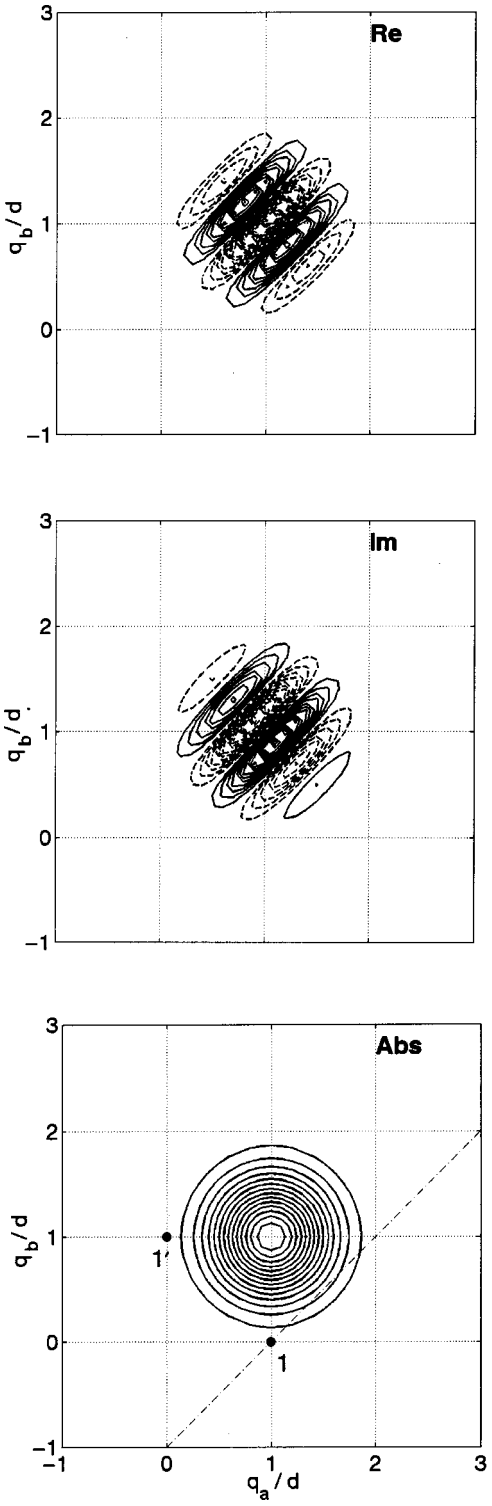

FIG. 9. Real part, imaginary part, and absolute value of the reference wave packet for the downhill case at $(t_p,t_d)_{\max}=(0.75,1.25)\tau_{\rm vib}$. Note the quasiclassical coherent-state structure of the reference wave packet. Plotting parameters are the same as in Fig. 7.

$$t_p+t_d=(n+\alpha)\tau_{\rm vib}. \tag{40}$$

This time can be sufficiently short (e.g., for $n=0$) that the nonecholike signal arising from the overlap in Eq. (38) would *not* be suppressed by inhomogeneous dephasing.

D. Related theoretical work

Szöcs *et al.*[66] very recently made a theoretical study of 2D photon echo spectroscopy on an excitonic two-site model system somewhat related to the present investigation. As a step toward a full analysis of vibrational and electronic coherence effects in photon echo signals from conjugated polymers, they considered the frequency resolved time-dependent third-order polarization from a purely electronic equal-energy two-site (four-level) system. The formal treatment and specializing conditions differ in several respects from those adopted here. Szöcs *et al.* found that the positions of off-diagonal peaks in the frequency domain interferogram carry information on the energy-transfer coupling strength, the relative heights of four characteristic peaks reflect the angle between the site-localized transition dipole moments, and the peak shapes depend on the ratio of homogeneous to inhomogeneous dephasing. Consistent with the conclusions of the present study, they concluded that the (heterodyne detected) frequency domain signal carried more structural and dynamical information than its (homodyne detected) time-domain counterpart.

In an earlier and more general study, Zhang *et al.*[39] also analyzed two-dimensional electronic spectroscopy from small aggregates coupled to a vibrational bath. Like those of Szöcs *et al.*,[66] the specializing conditions of Zhang *et al.* are rather different from ours, and the possibility of coherent vibrational motion is suppressed. Emphasizing the structural information content of these methods, they showed how various 2D techniques could provide information on intermolecular coupling strengths and patterns. Their study did not dwell explicitly on the possibility of separately addressing donor and acceptor moieties with differently polarized pulses.[67] Interestingly, Appendix F of Ref. 39 contains expressions for the contributions to various 2D four-wave mixing signal of first order in the electronic coupling constant J.

E. Relationship to time-resolved CARS

Nonlinear wave packet interferometry measurements of the kind suggested here and elsewhere[24,25] share some experimental and theoretical features with ultrafast time-resolved coherent anti-Stokes–Raman scattering measurements recently made by Karavistas *et al.*[17] The tr-CARS measurements did not involve electronic energy transfer, but—like wave packet interferometry—are sensitive to coherently excited electronic transitions and nuclear dynamics in a low-temperature medium (I_2 in an cryogenic argon matrix), where quantum mechanical wave packet motion is observed to play a significant role. Similar samples, along with molecular beams, could naturally be studied by wave packet intereferometry measurements as well.

Electronic dephasing (or decoherence) effects of the kind observed by time-resolved CARS will undoubtedly come into play in nonlinear wave packet interferometry measurements as well. Because of the nearly harmonic nature of low temperature host lattices, both time-resolved CARS and wave packet interferometry experiments on chromophores in solid matrices should be valuable testing grounds for quantitative models of electronic decoherence.[68–70]

F. Concluding remarks

Our analysis of nonlinear wave packet interferometry for an energy-transfer complex illustrates the potential power of this form of multidimensional electronic spectroscopy for observing coupled electronic and nuclear dynamics of many-body condensed molecular systems at the amplitude level. Our calculations for a simple model complex show that this form of ultrafast multidimensional electronic spectroscopy—along with the tools of polarization spectroscopy and optical phase control—has the capacity to measure not just the evolution of electronic populations and nuclear probability densities, but the time development of nuclear wave functions accompanying energy-transfer surface-crossing transitions.

Further research along the lines initiated here can address the important issues of multiple intra- and intermolecular modes, electronic dephasing, thermal effects, orientational disorder, and for gas phase samples, rotational dynamics and congestion. The neglect of vibrational dissipation specifically, a prerequisite for the onset of incoherent energy transfer as described by Förster theory, is in keeping with our specialization to very short-time dynamics (i.e., before the initial nonequilibrium vibrational distribution in the donor-excited state has decayed to quasithermal equilibrium). The amplitude-level dynamics studied here may no longer be readily discernible once the regime of Förster transfer ensues, but wave packet interferometry could be a sensitive means for observing the *onset* of incoherent hopping and the decay of donor–acceptor electronic coherence with increasing transfer intervals. In this connection it is worth mentioning that while the treatment given in this paper is based on a pure-state description of the energy-transfer complex, the approach is also directly applicable to isolated or condensed-phase systems with population distributed over thermally occupied levels. This generalization is accomplished formally by the elementary step of summing with Boltzmann weight over the initially populated energy states of the complex plus bath.[21]

In the interest of conceptual and computational simplicity, we here assumed weak energy-transfer coupling (J less than ω). Weak coupling should not be a requirement for interwell coherence to be observed by wave packet interferometry, however, and it might be anticipated that stronger coupling would lead to more intense (if less simply interpretable) interference spectroscopy signals. Further numerical studies of wave packet interferometry in the strong and intermediate coupling regimes will be a natural topic for future research. Since the numerical calculations reported here (but not the basic theoretical expressions) use laser pulses that are arbitrarily abrupt on the vibrational time scale, it will be necessary to further investigate the practical consequences of nonzero pulse duration and finite spectral bandwidth. We have specialized to pulse sequences with a few specific polarization combinations that are sensitive to the nuclear wave function arising from energy transfer to the acceptor-excited potential energy surface. Future studies can include pulse sequences of arbitrary polarization.[71]

APPENDIX A: ALTERNATIVE POLARIZATIONS

Here we summarize the interference signal under alternative polarization conditions for the oriented model system considered in Sec. III. Under polarizations $A_xB_yC_xD_x$, the amplitude in the acceptor-excited state through first order in J becomes

$$\begin{aligned}|\psi_{1'}(t)\rangle = &|(B_y)_{1'}\rangle + |(JA_x)_{1'}\rangle + |(JC_x)_{1'}\rangle + |(JD_x)_{1'}\rangle \\ &+ |(D_xC_xB_y)_{1'}\rangle + |(D_xB_yA_x)_{1'}\rangle \\ &+ |(C_xB_yA_x)_{1'}\rangle + |(JD_xC_xA_x)_{1'}\rangle \\ &+ |(D_xC_xJA_x)_{1'}\rangle \end{aligned} \tag{A1}$$

[compare Eq. (19)]. The four-pulse contribution to $\langle\psi_{1'}(t)|\psi_{1'}(t)\rangle$ gives the interference signal

$$\begin{aligned}P_{1'}(A_xB_yC_xD_x) = 2\,\mathrm{Re}\{&\langle(B_y)_{1'}|(JD_xC_xA_x)_{1'}\rangle \\ &+ \langle(B_y)_{1'}|(D_xC_xJA_x)_{1'}\rangle \\ &+ \langle(D_xC_xB_y)_{1'}|(JA_x)_{1'}\rangle \\ &+ \langle(D_xB_yA_x)_{1'}|(JC_x)_{1'}\rangle \\ &+ \langle(C_xB_yA_x)_{1'}|(JD_x)_{1'}\rangle\}, \end{aligned} \tag{A2}$$

which can be compared to Eq. (20). As in Sec. III, we can identify the optical phase-structure of the terms in Eq. (A2) in order to determine which portions of the signal are isolable by phase cycling. The last two overlaps in curly braces are not phase locked because the pulses within each pair induce transitions in the same direction in one of the overlapped states or in opposite directions in each of the overlapped states [e.g., in the fourth overlap of Eq. (A2), A_x and B_y both induce upward transitions in the three-pulse wave packet, while C_x drives an upward transition in the one-pulse wave packet and D_x drives a downward transition in the three-pulse wave packet]. The last two overlaps in Eq. (A2) are therefore expected to average to zero over many repetitions, and the signal becomes

$$\begin{aligned}P_{1'}(\phi_p,\phi_d) = 2\,\mathrm{Re}\{&\exp(i\phi_p - i\phi_d) \\ &\times(\langle(B_y)_{1'}|(JD_xC_xA_x)_{1'}\rangle^{(0)} \\ &+ \langle(D_xC_xB_y)_{1'}|(JA_x)_{1'}\rangle^{(0)}) \\ &+ \exp(i\phi_p + i\phi_d) \\ &\times\langle(B_y)_{1'}|(D_xC_xJA_x)_{1'}\rangle^{(0)}\}, \end{aligned} \tag{A3}$$

under $A_xB_yC_xD_x$ polarization [compare Eq. (22)]. Again it proves possible to isolate a single overlap, $\langle(B_y)_{1'}|(D_xC_xJA_x)_{1'}\rangle^{(0)}$, by combining signals with different intrapulse-pair phase shifts. In the single overlap isolable from Eq. (A3), electronic energy transfer takes place during the interval $t_p + t_w$; this differs slightly from the situation with Eq. (24). More significantly, as is discussed in Sec. V, the overlap isolable from Eq. (A3) may exhibit nonecholike behavior under some regimes of inhomogeneous broadening, an issue that could be the subject of an in-depth investigation.

For the two remaining polarization combinations, no single overlap is strictly isolable by phase cycling. With polarizations $A_xB_xC_yD_x$, the quadrilinear portion of the energy-transfer signal becomes

$$\begin{aligned}P_{1'}(\phi_p,\phi_d)=2\,\mathrm{Re}\{&\exp(i\phi_p-i\phi_d)\\&\times(\langle(C_y)_{1'}|(JD_xB_xA_x)_{1'}\rangle^{(0)}\\&+\langle(D_xC_yB_x)_{1'}|(JA_x)_{1'}\rangle^{(0)})\\&\times\exp(-i\phi_p-i\phi_d)\\&\times(\langle(D_xC_yA_x)_{1'}|(JB_x)_{1'}\rangle\\&+\langle(C_yB_xA_x)_{1'}|(JD_x)_{1'}\rangle^{(0)})\}.\end{aligned}\tag{A4}$$

And finally, under polarization $A_xB_xC_xD_y$, we find

$$\begin{aligned}P_{1'}(\phi_p,\phi_d)=2\,\mathrm{Re}\{&\exp(i\phi_p+i\phi_d)\\&\times(\langle(D_y)_{1'}|(JC_xB_xA_x)_{1'}\rangle^{(0)}\\&+\langle(D_y)_{1'}|(C_xB_xJA_x)_{1'}\rangle^{(0)})\\&\times\exp(-i\phi_p+i\phi_d)\\&\times(\langle(D_yC_xA_x)_{1'}|(JB_x)_{1'}\rangle^{(0)}\\&+\langle(D_yB_xA_x)_{1'}|(JC_x)_{1'}\rangle^{(0)})\}.\end{aligned}\tag{A5}$$

When (for which interpulse delays, if any) a sum of two overlaps in Eq. (22), (A3), (A4), or (A5) that is isolable by phase cycling reduces to a single overlap can only be determined by a detailed analysis of the nuclear dynamics.[72]

Let us consider the wave packet dynamics associated with the single overlap, $\langle(B_y)_{1'}|(D_xC_xJA_x)_{1'}\rangle^{(0)}$, that is isolable by combining signals (A3) with different phase locking angles. This overlap is equivalent to that between reference and target wave packets resulting from the sequences of electronic transitions

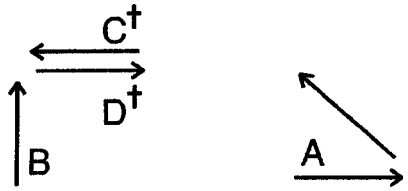

(A6)

respectively. Phase-space diagrams for the reference packet can be drawn which are analogous to those in Figs. 2 and 3. If we specialize to the case with energy-transfer interval $t_p+t_w=\tau_{\mathrm{vib}}/2$ just large enough to ensure one crossing of the donor–acceptor intersection, then coincidence between target and reference phase-points requires

$$t_p=\alpha\frac{\tau_{\mathrm{vib}}}{2},\quad t_w=(1-\alpha)\frac{\tau_{\mathrm{vib}}}{2},\quad t_d=\left(n+\frac{\alpha}{2}\right)\tau_{\mathrm{vib}}.\tag{A7}$$

APPENDIX B: TARGET AND REFERENCE WAVE PACKETS

Here we derive analytic expressions for the target (reference) wave packet defined by Eq. (25) [Eq. (26)]. Using the short-pulse limit of the B_x pulse propagator (11) and the free-evolution operator of first-order in J given in Ref. 52, we find

$$|\xi_{1'}\rangle=\frac{\mu J}{2}\,\mathrm{area}_B\int_0^{t_w}d\tau e^{-iH_{1'}(t_w-\tau)}e^{-iH_1\tau}|0,0\rangle.\tag{B1}$$

The target wave packet (B1) is assumed to originate from the vibrational ground state of the electronically unexcited complex; $\mathrm{area}_I=\int dt\,A_I(t)$ is the integrated pulse envelope.

We can use harmonic-oscillator creation and annihilation operators to go further with Eq. (B1). Adopting the usual definitions $q_a=(2m\omega)^{-1/2}(a^\dagger+a)$, $p_a=i(m\omega/2)^{1/2}(a^\dagger-a)$, $q_b=(2m\omega)^{-1/2}(b^\dagger+b)$, $p_b=i(m\omega/2)^{1/2}(b^\dagger-b)$, and introducing the corresponding phase-space translation operators $T_a(\alpha)=\exp(\alpha a^\dagger-\alpha^* a)$ and $T_b(\beta)=\exp(\beta b^\dagger-\beta^* b)$,[73] we have

$$H_1=T_a(\delta)(H_0+\epsilon_1)T_a^\dagger(\delta),\tag{B2}$$

$$H_{1'}=T_b(\delta)(H_0+\epsilon_{1'})T_b^\dagger(\delta),\tag{B3}$$

$$H_2=T_a(\delta)T_b(\delta)(H_0+\epsilon_2)T_b^\dagger(\delta)T_a^\dagger(\delta).\tag{B4}$$

From relations (B1)–(B4) and some operator algebra[73] it follows that

$$\begin{aligned}|\xi_{1'}\rangle=-\frac{\mu J}{2}\,\mathrm{area}_B e^{-2\delta^2-i\epsilon_1\tau_{\mathrm{vib}}/2}&\\\times\int_0^{\tau_{\mathrm{vib}}/2}d\tau\exp\{&i(\epsilon_{1'}-\epsilon_1)\tau-2i\delta^2\sin\omega\tau\\&+\delta(1-e^{i\omega\tau})a^\dagger\\&+\delta(1+e^{i\omega\tau})b^\dagger\}|0,0\rangle.\end{aligned}\tag{B5}$$

The dimensionless displacement is $\delta=(m\omega/2)^{1/2}d$, and the waiting time has been set to $t_w=\tau_{\mathrm{vib}}/2$.

In the short-pulse limit, the reference wave packet (26) prepared from the vibronic ground state remains a quasiclassical coherent state of the form

$$\begin{aligned}|\alpha_{1'}\rangle=-i\left(\frac{\mu}{2}\right)^3\mathrm{area}_A\,\mathrm{area}_C\,\mathrm{area}_D\,e^{i\Omega_pt_p-i\Omega_dt_d}e^{iH_2t_d}&\\\times e^{-iH_{1'}(t_p+t_w+t_d)}e^{iH_0t_p}|0,0\rangle.\end{aligned}\tag{B6}$$

Relations (B3) and (B4) plus some operator manipulations (and the choice $t_w=\tau_{\mathrm{vib}}/2$) lead to the more explicit expression

$$\begin{aligned}|\alpha_{1'}\rangle=i\left(\frac{\mu}{2}\right)^3\mathrm{area}_A\,\mathrm{area}_C\,\mathrm{area}_D\exp\Bigg\{&-i\frac{\epsilon_{1'}\tau_{\mathrm{vib}}}{2}\\&+i(\Omega_p-\epsilon_{1'})t_p-i(\Omega_d+\epsilon_{1'}-\epsilon_2)t_d+\delta^2e^{i\omega t_d}\\&-\delta^2e^{-i\omega t_p}-2\delta^2+\delta(1-e^{i\omega t_d})a^\dagger\\&+\delta(1+e^{-i\omega t_p})b^\dagger\Bigg\}|0,0\rangle.\end{aligned}\tag{B7}$$

The inner product of Eqs. (B5) and (B7) leads to the experimentally isolable complex overlap, Eq. (29), that is plotted in Sec. IV.

APPENDIX C: INTERFEROGRAM FRINGE STRUCTURE

In order to better understand the local fringe structure of the peaks in the 2D interferograms presented in Sec. IV, it is useful to consider the first derivatives with respect to t_p and t_d of the complex overlap between the target (25) and reference (26) wave packets. In the short-pulse limit adopted there, the reference wave packet (though not the target) prepared from the vibrational ground state is a minimum-uncertainty Gaussian wave packet,[74]

$$\langle q_a, q_b|\alpha_{1'}\rangle = \exp\left\{ -\frac{m\omega}{2}(q_a-\overline{q_a})^2 - \frac{m\omega}{2}(q_b-\overline{q_b})^2 + i\overline{p_a}(q_a-\overline{q_a}) + i\overline{p_b}(q_b-\overline{q_b}) + i\gamma \right\}, \tag{C1}$$

whose time evolution is governed by the quasiclassical motion of the average values of the position and momentum expectation values

$$\overline{q_a} \equiv \frac{\langle\alpha_{1'}|q_a|\alpha_{1'}\rangle}{\langle\alpha_{1'}|\alpha_{1'}\rangle} = d(1-\cos\omega t_d), \tag{C2}$$

$$\overline{p_a} \equiv \frac{\langle\alpha_{1'}|p_a|\alpha_{1'}\rangle}{\langle\alpha_{1'}|\alpha_{1'}\rangle} = -m\omega d\sin\omega t_d, \tag{C3}$$

$$\overline{q_b} \equiv \frac{\langle\alpha_{1'}|q_b|\alpha_{1'}\rangle}{\langle\alpha_{1'}|\alpha_{1}\rangle} = d(1-\cos\omega(t_w+t_p)), \tag{C4}$$

$$\overline{p_b} \equiv \frac{\langle\alpha_{1'}|p_b|\alpha_{1'}\rangle}{\langle\alpha_{1'}|\alpha_{1'}\rangle} = m\omega d\sin\omega(t_w+t_p), \tag{C5}$$

and the (complex) phase

$$\gamma = \gamma_0 - \frac{\pi}{2} - i\ln\left\{\left(\frac{\mu}{2}\right)^3 \text{area}_A\ \text{area}_C\ \text{area}_D\right\} + \Omega_p t_p - \Omega_d t_d + \phi_p - \phi_d - \omega t_w - \epsilon_{1'}(t_d+t_w+t_p) + \epsilon_2 t_d + \frac{m\omega d^2}{4}(\sin 2\omega t_d - \sin 2\omega(t_w+t_p)). \tag{C6}$$

Contributions from the short-pulse limit of the pulse propagators (11) have been included in Eq. (C6); γ_0 is the arbitrary initial phase attached to $\langle q_a, q_b|n_0\rangle$. The wave function (C1) is the position-space representation of Eq. (B7).

Writing the target-reference overlap in terms of a complex phase, $\langle\alpha_{1'}|\xi_{1'}\rangle = \exp(i\Gamma)$, leads to the sought-for time derivatives

$$\frac{\partial\Gamma}{\partial t_p} = -\Omega_p + \epsilon_{1'} + \frac{m\omega^2 d^2}{2} - m\omega^2 d e^{i\omega(t_w+t_p)}\frac{\langle\alpha_{1'}|q_b-\overline{q_b}|\xi_{1'}\rangle}{\langle\alpha_{1'}|\xi_{1'}\rangle}, \tag{C7}$$

$$\frac{\partial\Gamma}{\partial t_d} = \Omega_d + \epsilon_{1'} - \epsilon_2 - \frac{m\omega^2 d^2}{2} + m\omega^2 d e^{-i\omega t_d}\frac{\langle\alpha_{1'}|q_a-\overline{q_a}|\xi_{1'}\rangle}{\langle\alpha_{1'}|\xi_{1'}\rangle}. \tag{C8}$$

As could have been anticipated from Fig. 3, the derivative with respect to $t_d(t_p)$ is sensitive to only the donor (acceptor) vibration. The interferogram fringe structure yields information on the spatial form of the target energy-transfer amplitude through the last term on the right-hand side of Eqs. (C7) and (C8).

Our closed-form expression for $\langle\alpha_{1'}|\xi_{1'}\rangle$ gives equivalent alternative forms for the delay derivatives of Γ. By differentiation of Eq. (29) we obtain

$$\frac{\partial\Gamma}{\partial t_p} = -i\frac{\partial\langle\alpha_{1'}|\xi_{1'}\rangle/\partial t_p}{\langle\alpha_{1'}|\xi_{1'}\rangle} = -\Omega_p + \epsilon_{1'} + \omega\delta^2 e^{i\omega t_p} R \tag{C9}$$

and

$$\frac{\partial\Gamma}{\partial t_d} = -i\frac{\partial\langle\alpha_{1'}|\xi_{1'}\rangle/\partial t_d}{\langle\alpha_{1'}|\xi_{1'}\rangle} = \Omega_d + \epsilon_{1'} - \epsilon_2 - \omega\delta^2\epsilon^{-i\omega t_d} R \tag{C10}$$

where, in both cases,

$$R = \frac{\int_0^{\tau_{\text{vib}}/2} d\tau \exp\{i(\epsilon_{1'}-\epsilon_1+\omega)\tau + \delta^2 e^{i\omega\tau}(e^{i\omega t_p}+e^{-i\omega t_d}-1) + \delta^2 e^{-i\omega\tau} - 2\delta^2\}}{\int_0^{\tau_{\text{vib}}/2} d\tau \exp\{i(\epsilon_{1'}-\epsilon_1)\tau + \delta^2 e^{i\omega\tau}(e^{i\omega t_p}+e^{-i\omega t_d}-1) + \delta^2 e^{-i\omega\tau} - 2\delta^2\}}. \tag{C11}$$

Since the same ratio R appears in both Eqs. (C9) and (C10), and the integrand in the numerator of Eq. (C11) simply contains an extra factor $\exp(i\omega\tau)$, we have the remarkable result

$$\frac{e^{i\omega(t_p+t_d)}}{\omega\delta^2}\left(\Omega_d + \epsilon_{1'} - \epsilon_2 + i\frac{\partial}{\partial t_d}\right)\langle\alpha_{1'}|\xi_{1'}\rangle_{\epsilon_1\epsilon_{1'},\epsilon_2} = \frac{1}{\omega\delta^2}\left(\Omega_p + \epsilon_{1'} - i\frac{\partial}{\partial t_p}\right)\langle\alpha_{1'}|\xi_{1'}\rangle_{\epsilon_1,\epsilon_{1'}\epsilon_2} = \langle\alpha_{1'}|\xi_{1'}\rangle_{\epsilon_1,\epsilon_{1'}+\omega,\epsilon_2+\omega}. \tag{C12}$$

The rate of change of the interferogram along either time axis specifies the complex-valued interference signal from a *different energy-transfer complex* with the acceptor and two-exciton site energies increased by one vibrational quantum. We have used the first equality in Eq. (C12) as a consistency check on the t_p and t_d fringe structure of the calculated interferograms presented in Sec. IV.

ACKNOWLEDGMENTS

One of the authors (J.A.C.) thanks Rick Dahlquist, University of Oregon, for encouraging him to consider optical phase cycling in the context of wave packet interferometry; Howard Carmichael, Oregon, and Sid Nagel, The University of Chicago, for helping him understand harmonic oscillators; and David Jonas, University of Colorado, for asking about the observability of the phase change associated with energy transfer mentioned in Ref. 52. Chris Bardeen, University of Illinois, kindly brought the work of Ref. 46 to our attention. We benefited from many helpful conversations with Professor Tom Dyke and Professor Andy Marcus, UO, who are presently attempting experiments along the lines discussed here. This work was supported by a grant from the US National Science Foundation. Additional support from the UO Department of Chemistry and Oregon Center for Optics is gratefully acknowledged.

[1] N. F. Scherer, R. Carlson, A. Matro, M. Du, A. J. Ruggiero, V. Romero-Rochin, J. A. Cina, G. R. Fleming, and S. A. Rice, J. Chem. Phys. **95**, 1487 (1991).
[2] N. F. Scherer, A. Matro, R. J. Carlson, M. Du, L. D. Ziegler, J. A. Cina, and G. R. Fleming, J. Chem. Phys. **96**, 4180 (1992).
[3] A. W. Albrecht, J. D. Hybl, S. M. Gallagher Faeder, and D. M. Jonas, J. Chem. Phys. **111**, 10934 (1999); **115**, 5691 (2001).
[4] W. P. de Boeij, M. S. Pshenichnikov, and D. A. Wiersma, Chem. Phys. **233**, 287 (1998).
[5] L. Lepetit and M. Joffre, Opt. Lett. **21**, 564 (1996).
[6] J. D. Hybl, A. Albrecht Ferro, and D. M. Jonas, J. Chem. Phys. **115**, 6606 (2001).
[7] A. H. Zewail, Science **242**, 1645 (1988).
[8] A. A. Mokhtari and J. Chesnoy, IEEE J. Quantum Electron. **25**, 2528 (1989); P. F. Barbara and W. Jarzeba, Adv. Photochem. **15**, 1 (1990); R. Jimenez, G. R. Fleming, P. V. Kumar, and M. Maroncelli, Nature (London) **369**, 471 (1994); M. Chattoraj, B. A. King, G. U. Bublitz, and S. G. Boxer, Proc. Natl. Acad. Sci. U.S.A. **93**, 8362 (1996).
[9] L. W. Ungar and J. A. Cina, Adv. Chem. Phys. **100**, 171 (1997).
[10] See also S. Saikan, T. Nakabayashi, Y. Kanematsu, and N. Tato, Phys. Rev. B **38**, 7777 (1988); W. H. Hesselink and D. A. Wiersma, Phys. Rev. Lett. **43**, 1991 (1979).
[11] M. C. Beard, G. M. Turner, and C. A. Schmuttenmaer, J. Am. Chem. Soc. **122**, 11541 (2000); O. Golonzka, M. Khalil, N. Demirdöven, and A. Tokmakoff, J. Chem. Phys. **115**, 10814 (2001); M. Zanni, N.-H. Ge, Y. S. Kim, and R. M. Hochstrasser, Proc. Natl. Acad. Sci. U.S.A. **98**, 11265 (2001).
[12] L. J. Kaufman, J. Heo, L. D. Ziegler, and G. R. Fleming, Phys. Rev. Lett. **88**, 207402 (2002); K. J. Kubarych, C. J. Milne, S. Lin, V. Astinov, and R. J. D. Miller, J. Chem. Phys. **116**, 2016 (2002).
[13] M. Cho, N. F. Scherer, G. R. Fleming, and S. Mukamel, J. Chem. Phys. **96**, 5618 (1992); S. Mukamel, *Principles of Nonlinear Optical Spectroscopy* (Oxford University Press, New York, 1995).
[14] Y. Tanimura and S. Mukamel, J. Chem. Phys. **99**, 9496 (1993).
[15] H. Metiu and V. Engel, J. Opt. Soc. Am. B **7**, 1709 (1990). See also W. S. Warren and A. H. Zewail, J. Chem. Phys. **78**, 2279 (1983); **78**, 2298 (1983).
[16] W. Domcke and G. Stock, Adv. Chem. Phys. **100**, 1 (1997); W. T. Pollard, S. L. Dexheimer, Q. Wang, L. A. Peteanu, C. V. Shank, and R. A. Mathies, J. Phys. Chem. **96**, 6147 (1992); D. M. Jonas, S. E. Bradforth, S. A. Passino, and G. R. Fleming, *ibid.* **99**, 2594 (1995); T. J. Smith, L. W. Ungar, and J. A. Cina, J. Lumin. **58**, 66 (1994); Z. Li, J. Fang, and C. C. Martens, J. Chem. Phys. **104**, 6919 (1996); C. J. Bardeen, J. Che, K. R. Wilson, V. V. Yakovlev, V. A. Apkarian, C. C. Martens, R. Zadoyan, B. Kohler, and M. Messina, *ibid.* **106**, 8486 (1997); Y.-S. Shen and J. A. Cina, *ibid.* **110**, 9793 (1999).
[17] M. Karavitas, R. Zadoyan, and V. A. Apkarian, J. Chem. Phys. **114**, 4131 (2001); see also I. Pinkas, G. Knopp, and Y. Prior, *ibid.* **115**, 236 (2001).
[18] E. J. Heller, J. Chem. Phys. **68**, 2066 (1978).
[19] E. J. Heller, R. L. Sundberg, and D. Tannor, J. Phys. Chem. **86**, 1822 (1982); J. L. McHale, Acc. Chem. Res. **34**, 265 (2001).
[20] S. Mukamel, J. Phys. Chem. **88**, 3185 (1984); Y. J. Yan and S. Mukamel, J. Chem. Phys. **88**, 5735 (1988).
[21] R. A. Harris, R. A. Mathies, and W. T. Pollard, J. Chem. Phys. **85**, 3744 (1986).
[22] A more general approach based on a moment expansion of physical observables, but independent of a Gaussian ansatz on the wave function or density matrix, has been recently put forward by O. V. Prezhdo and Y. V. Pereverzev, J. Chem. Phys. **113**, 6557 (2000); **116**, 4450 (2002).
[23] See also D. J. Tannor, *Introduction to Quantum Mechanics: A Time Dependent Perspective* (University Science Books, New York, 2003).
[24] J. A. Cina and R. A. Harris, J. Chem. Phys. **100**, 2531 (1994); Science **267**, 832 (1995). See also R. P. Duarte-Zamorano and V. Romero-Rochín, J. Chem. Phys. **114**, 9276 (2001); C. S. Maierle and R. A. Harris, *ibid.* **109**, 3713 (1998).
[25] J. A. Cina, J. Chem. Phys. **113**, 9488 (2000).
[26] T. S. Humble and J. A. Cina, Bull. Korean Chem. Soc. (to be published).
[27] D. J. Tannor and S. A. Rice, J. Chem. Phys. **83**, 5013 (1985); J. Cao, J. Lumin. **87–89**, 30 (2000); R. J. Levis, G. M. Menkir, and H. Rabitz, Science **292**, 709 (2001).
[28] R. Zadoyan, D. Kohen, D. A. Lidar, and V. A. Apkarian, Chem. Phys. **266**, 323 (2001).
[29] R. van Grondelle, J. P. Dekker, T. Gillbro, and V. Sundstrom, Biochim. Biophys. Acta **1187**, 1 (1994); X. Hu and K. Shulten, Phys. Today **50**, 28 (1997).
[30] *J-Aggregates*, edited by T. Kobayashi (World Scientific, Singapore, 1996).
[31] H. S. Cho, D. H. Jung, M.-C. Yoon *et al.*, J. Phys. Chem. A **105**, 4200 (2001); C.-K. Min, T. Joo, M.-C. Yoon, C. M. Kim, Y. N. Hwang, D. Kim, N. Aratani, N. Yoshida, and A. Osuka, J. Chem. Phys. **114**, 6750 (2001).
[32] F. Zhu, C. Galli, and R. M. Hochstrasser, J. Chem. Phys. **98**, 1042 (1993); erratum, **98**, 9222 (1993).
[33] A. Albrecht Ferro and D. M. Jonas, J. Chem. Phys. **115**, 6281 (2001).
[34] Y. Sakata, T. Toyoda, T. Yamazaki, and I. Yamazaki, Tetrahedron Lett. **33**, 5077 (1992); J. A. Pescatore and I. Yamazaki, J. Phys. Chem. **100**, 13333 (1996).
[35] Th. Förster, in *Modern Quantum Chemistry*, Part III, edited by O. Sinanoglu (Academic, New York, 1965), p. 93.
[36] S. Rackovsky and R. Silbey, Mol. Phys. **25**, 61 (1973).
[37] T. F. Soules and C. B. Duke, Phys. Rev. A **3**, 262 (1971).
[38] For a recent relaxation-theory study of vibrational effects in electronic energy transfer see M. Yang and G. R. Fleming, Chem. Phys. **275**, 355 (2002).
[39] W. M. Zhang, V. Chernyak, and S. Mukamel, J. Chem. Phys. **110**, 5011 (1999); see also V. Chernyak, W. M. Zhang, and S. Mukamel, *ibid.* **109**, 9587 (1998).
[40] A. J. Leggett, S. Chakravarty, A. T. Dorsey, M. P. A. Fisher, A. Garg, and W. Zwerger, Rev. Mod. Phys. **59**, 1 (1987); our reference is to a statement on p. 15 to the effect that for practical purposes, only the population difference between the two [electronic] states was then accessible in realistic experiments.
[41] In our numerical calculations, ϵ_2 is taken to *equal* $\epsilon_1+\epsilon_{1'}$ unless otherwise stated.
[42] John Jean investigated the short-pulse-driven dynamics of a similar system in contact with a thermal reservoir in a ground-breaking study of the competition between coherence and relaxation in wave packet surface crossing: J. M. Jean, J. Phys. Chem. A **102**, 7549 (1998). See also A. Matro and J. A. Cina, J. Phys. Chem. **99**, 2568 (1995); C. Kalyanaraman and D. G. Evans, J. Chem. Phys. **115**, 7076 (2001).
[43] For plots of the adiabatic potential energy surfaces of this model under strong and weak coupling, see Fig. 2 of Förster's article (Ref. 35).
[44] In the case of equal site energies, $\epsilon_1=\epsilon_{1'}$, the intersection between donor and acceptor surfaces includes $q_b=q_a=0$, so energy transfer proceeds efficiently at the Franck–Condon point. When $\epsilon_1=\epsilon_{1'}+m\omega^2d^2=\epsilon_{1'}+2E_{\mathrm{FC}}$, the acceptor surface passes through the donor minimum; for continuous spectra this would be the case of maximal "Förster overlap" between donor emission and acceptor absorption. A further redshift in the acceptor absorption spectrum would lead to an inverted regime of decreasing energy-transfer efficiency.
[45] The lower-case subscripts designate "preparation," "waiting," and "delay."
[46] Experiments on fluorescence detection of femtosecond accumulated photon echoes have measured a similar quantity that is quadrilinear in the field amplitudes of phase-related continuous wave beams. The time resolution in those experiments was set by the field correlation time of a continuous-wave laser rather than the pulse duration. See K. Uchikawa, H.

Ohsawa, T. Suga, and S. Saikan, Opt. Lett. **16**, 13 (1991); S. Saikan, K. Uchikawa, and H. Ohsawa, *ibid.* **16**, 10 (1991).

[47] We set $\hbar=1$ throughout this paper.

[48] We specify the arbitrary initial phase so that, $[t_A-t_0]|\Psi(t_0)\rangle=|0\rangle|n_0\rangle$, where $|n_0\rangle$ is a vibrational eigenket of H_0 with energy E_{n_0}.

[49] As defined here, the pulse propagators are anti-Hermitian: $I^\dagger=-I$.

[50] Under these approximations, the integrand of Eq. (11) becomes $[-\tau+t_I]V_I(\tau)[\tau-t_I]\cong\{[-(\mu_a\cdot e_I)/2](|1\rangle\langle 0|e^{-iH_1(t_I-\tau)}e^{iH_0(t_I-\tau)}+|2\rangle\times\langle 1'|e^{-iH_2(t_I-\tau)}e^{iH_{1'}(t_I-\tau)})-[(\mu_b\cdot e_I)/2](|1'\rangle\langle 0|e^{-iH_{1'}(t_I-\tau)}e^{iH_0(t_I-\tau)}+|2\rangle\langle 1|e^{-iH_2(t_I-\tau)}e^{iH_1(t_I-\tau)})\}A_I(\tau-t_I)e^{-i\Omega_I(\tau-t_I)-i\Phi_I}+\text{H.c.}$

[51] The expression for $|\psi_1\rangle$ is the same as Eq. (12), but with $\langle 1|$ instead of $\langle 1'|$ on the right-hand side. The nuclear wave function in the bi-excitonic state is given by $|\psi_2\rangle=\langle 2|[t-t_D]\{D[t_d]C[t_w+t_p]+D[t_d+t_w]B[t_p]+[t_d]C[t_w]B[t_p]+D[t_d+t_w+t_p]A+[t_d]C[t_w+t_p]A+[t_d+t_w]B[t_p]A+D[t_d]C[t_w]B[t_p]A\}|0\rangle|n_0\rangle$.

[52] Where $[t]_0=\exp(-iHt)|_{J=0}$ and $[t]_1=-iJ\int_0^t d\tau\{|1'\rangle\exp(-iH_{1'}(t-\tau))\exp(-iH_1\tau)\langle 1|+|1\rangle\exp(-iH_1\tau)\exp(-iH_{1'}(t-\tau))\langle 1'|\}$. Notice that the first-order evolution operator carries a phase factor $-i=e^{-i\pi/2}$ associated with the energy-transfer process, which our amplitude-sensitive measurements will be able to detect.

[53] An experimental strategy for isolating the interference contribution to the population of a given electronic state with beam choppers and lock-in amplifiers was demonstrated in Refs. 1 and 2.

[54] We use notation in which a bra retains the name of the ket to which it is dual: $\langle BA|$ is the bra dual to the ket $|BA\rangle$.

[55] Through the pulse propagators (11), which involve the dot products $\boldsymbol{\mu}_a\cdot\mathbf{e}_I$ and $\boldsymbol{\mu}_b\cdot\mathbf{e}_I$.

[56] P. Andrews and W. L. Barnes, Science **290**, 785 (2000).

[57] In the phase-locking scheme of Scherer and co-workers (Refs. 1 and 2), the pulses in a phase-locked pair differ by a pure delay, and are otherwise exact copies of each other. For example, the phases-at-arrival Φ_A and Φ_B differ at most by an integer multiple of 2π. In that method, the intrapulse-pair delays (t_p) are actively stabilized and selectively undersampled so that $\Phi_B-\Phi_A=2\pi N=\Omega_p t_p+\phi_p$ for a chosen value of the locking angle ϕ_p. The same situation applies for the *CD* pulse pair. With respect to the *interpulse-pair* phase shifts, timing jitter on the unstabilized delay t_w allows us to regard the interpulse-pair phase shifts as random variables. For a detailed discussion of the relationship between phase shifts and time delays, see Ref. 3.

[58] D. Keusters, H.-S. Tan, and W. S. Warren, J. Phys. Chem. A **103**, 10369 (1999); D. Keusters, P. Tian, and W. S. Warren, in The *Thirteenth International Conference on Ultrafast Phenomena*, OSA Trends in Optics and Photonics, Vol. 72, OSA Technical Digest, Postconference Edition (Optical Society of America, Washington, D.C., 2002), pp. 480–481.

[59] A rudimentary example of phase-cycling in linear ultrafast spectroscopy can be found in Ref. 2. There it was shown that in-phase and in-quadrature interferograms could be combined to yield the resonant part of the time-dependent linear dipole susceptibility.

[60] It may be noted that while the overlaps in Eq. (23) depend explicitly on the observation time t, the isolable single overlap in Eq. (24) is t-independent. In both contributions to Eq. (23), one of the overlapped wave packets evolves after t_D with a time evolution operator zeroth order in J and the other with an operator linear in J. In the overlap (24) on the other hand, both wave packets experience evolution after t_D under the same unitary operator $[t-t_D]_0$ [see Eq. (13)]; so their overlap does not change. It happens similarly, that the single overlap isolable with $A_xB_yC_xD_x$ polarization (see Appendix A) is observation-time independent. For both polarization combinations, however, it may be desirable in cases of relatively strong energy-transfer coupling to time gate the measurement of acceptor-state population—on about a picosecond time scale—in order to ensure that the portion linear in J dominates the acceptor-state population.

[61] This result has the special implication that after $(1-\alpha)t_w$ of motion in the $1'$ state, the *a*-mode target trajectory reaches a phase-point lying on the Franck–Condon energy shell; the phase-space location of the target-state *a*-mode will hence be accessible to a reference wave packet after some t_d interval of (backwards) motion in state 2. This interesting elementary feature of the transferred amplitude's motion in an energy-transfer system does not seem to have been noted previously.

[62] The basic physics of this process is the same as follows the instantaneous upward displacement of the hanging point of a Hooke's law spring holding a stationary weight: If the hanging point is returned to its original position after $\alpha\tau_{\text{vib}}/2$, then $(1-\alpha)\tau_{\text{vib}}/2$ later, the mass passes downward through the same vertical position it had at time $\alpha\tau_{\text{vib}}/2$.

[63] Equation (29) was integrated with a time step $\tau_{\text{vib}}/2400$, yielding numerical errors of about a part in 10^6. The interference signals presented here supersede the preliminary calculations of D. Kilin and J. A. Cina, *Ultrafast Phenomena* (Springer, Berlin, in press), Vol. 13, conference proceedings. The latter calculations were performed less accurately, by numerical diagonalization of the one-exciton subspace in the presence of a small specified value for J.

[64] There does not appear to be any fundamental reason why fluorescence-detected wave packet interferometry signals could not be measured on single molecules; in which case the issue of inhomogeneous broadening would be moot if the site energies were stable for the duration of data acquisition.

[65] See Chap. 10 of Shaul Mukamel's book, cited in Ref. 13.

[66] V. Szöcs, T. Pálszegi, A. Torschanoff, and H. F. Kaufmann, J. Chem. Phys. **116**, 8218 (2002).

[67] This issue is addressed, however, by O. Golonzka and A. Tokmakoff, J. Chem. Phys. **115**, 297 (2001).

[68] J. A. Cina and R. A. Harris, *Ultrafast Phenomena IX*, edited by W. Knox and P. Barbara (Springer, Berlin, 1994), p. 486.

[69] R. Silbey and R. A. Harris, J. Phys. Chem. **93**, 7062 (1989).

[70] S. Jang, J. Cao, and R. J. Silbey, J. Chem. Phys. **116**, 2705 (2002).

[71] For instance, the uniformly polarized sequence $A_xB_xC_xD_x$ should reveal the loss of amplitude in a donor-state wave packet of order J^2 due to electronic energy transfer. The corresponding quadrilinear signal should be resistant to degradation by orientational disorder, and even provide useful amplitude-level information from a randomly oriented sample.

[72] The Appendix of Ref. 25 analyzed the dynamics underlying the *C* and *D* terms (in the notation of that paper) in the nonlinear interferogram for a polyatomic molecule that *does not* undergo energy transfer. Conditions were found under which these two terms do not coincide, and arguments made that under these same conditions, the *A* and *B* term signals would vanish except at very short t_w. It is worth noting that the *C* and *D* terms can more generally be separated from each other by phase cycling, which isolates $A+D$ and $B+C$. See Ref. 26.

[73] C. Cohen-Tannoudji, B. Diu, and F. Laloë, *Complement* G_V, *Quantum Mechanics Vol. I* (Wiley, New York, 1977).

[74] E. J. Heller, J. Chem. Phys. **62**, 1544 (1975).